NASA TECHNICAL NOTE

NASA TN D-6933

NASA TN D-6933

ON THE NUMERICAL SIMULATION OF THREE-DIMENSIONAL TRANSONIC FLOW WITH APPLICATION TO THE C-141 WING

by Harvard Lomax, Frank R. Bailey, and William F. Ballhaus

Ames Research Center
Moffett Field, Calif. 94035

NATIONAL AERONAUTICS AND SPACE ADMINISTRATION • WASHINGTON, D. C. • AUGUST 1973

1. Report No.	2. Government Accession No.	3. Recipient's Catalog No.
TN D–6933		

4. Title and Subtitle	5. Report Date
ON THE NUMERICAL SIMULATION OF THREE-DIMENSIONAL TRANSONIC FLOW WITH APPLICATION TO THE C-141 WING	August 1973
	6. Performing Organization Code

7. Author(s)	8. Performing Organization Report No.
Harvard Lomax, Frank R. Bailey, and William F. Ballhaus	A–4583

9. Performing Organization Name and Address	10. Work Unit No.
NASA–Ames Research Center Moffett Field, Calif. 94035	501–06–01–09–00–21
	11. Contract or Grant No.

12. Sponsoring Agency Name and Address	13. Type of Report and Period Covered
National Aeronautics and Space Administration Washington, D. C. 20546	Technical Note
	14. Sponsoring Agency Code

15. Supplementary Notes

16. Abstract

Results computed by a finite-difference, relaxation algorithm are presented for the supercritical flow ($M_\infty = 0.825$) about the C-141 airplane wing, which has sweep, taper, and twist. Comparisons with both wind-tunnel and flight data indicate that computed solutions of the classical transonic small disturbance equation can accurately simulate high Reynolds number flows when the shock sweep angle is small. It is also shown that this equation poorly approximates the complete potential equation when embedded shock waves are swept at angles greater than about 15°. Hence, a more consistent small disturbance equation is derived for use in more general cases.

17. Key Words (Suggested by Author(s))	18. Distribution Statement
Transonic flow C-141 wing Swept wing	Unclassified – Unlimited

19. Security Classif. (of this report)	20. Security Classif. (of this page)	21. No. of Pages	22. Price*
Unclassified	Unclassified	51	$3.00

* For sale by the National Technical Information Service, Springfield, Virginia 22151

ON THE NUMERICAL SIMULATION OF THREE-DIMENSIONAL TRANSONIC FLOW WITH APPLICATION TO THE C-141 WING

Harvard Lomax, Frank R. Bailey, and William F. Ballhaus

Ames Research Center

SUMMARY

Results computed by a finite-difference, relaxation algorithm are presented for the supercritical flow ($M_\infty = 0.825$) about the C-141 airplane wing, which has sweep, taper, and twist. Comparisons with both wind-tunnel and flight data indicate that computed solutions of the classical transonic small disturbance equation can accurately simulate high Reynolds number flows when the shock sweep angle is small. It is also shown that this equation poorly approximates the complete potential equation when embedded shock waves are swept at angles greater than about 15°. Hence, a more consistent small disturbance equation is derived for use in more general cases.

INTRODUCTION

Finite-difference calculations of inviscid, transonic flows about two-dimensional airfoils and axisymmetric bodies have been reported by several authors (see, e.g., refs. 1 through 5; these works are summarized in ref. 6). Results of these calculations agree well with experimental data under the following conditions: (1) the presence of wind-tunnel walls are included in the calculations; (2) viscous effects are considered.

The second condition depends on several others. First, the Reynolds number in the experiment must be high enough for the boundary layer (especially near shocks) to be thin. Second, the local Mach number upstream of a computed shock must be low enough to preclude shock-induced separation in the experiment ($M_1 \lesssim 1.3$). Third, adverse pressure gradients near the trailing-edge must be mild enough for the confinement of what separation there is to a small region near the trailing edge. Finally, because of the preceding condition, comparisons between experimental and computed results should be made at the same lift coefficient. Fortunately, transonic aircraft fly at high Reynolds numbers, and they are designed to maintain flow attachment over as much of the wing as possible. Hence, inviscid computational methods are applicable to a variety of practical flow situations.

One of the major problems facing aircraft designers today is the three-dimensional transonic interference problem. At transonic Mach numbers, three-dimensional effects due to the presence of a fuselage or wing tip can influence the flow field for large distances in the spanwise direction. Such flow fields, especially for low and moderate aspect ratio wings, are seldom close to two dimensional anywhere on the wing. It is pointed out, in references 14 and 15 (where the present method is

described in detail), that treatment of the three-dimensional transonic problem involves more than a trivial extension of existing two-dimensional methods. Some of the major complications are: (1) the circulation is a function of the spanwise coordinate and must be determined as part of the solution process; (2) stability can be difficult to maintain, especially in supersonic flow regions; (3) swept and tapered planform shapes complicate application of wing boundary conditions; and (4) shocks, which are nearly normal to the free-stream direction in two-dimensions, can be oblique in the lateral direction. Compounding the last complication is the fact that oblique shocks may be poorly alined with the coordinate system making them difficult to capture sharply.

The effect of shock angle on shock strength is the subject of part I of this report. A comparison of the complete potential equation with the classical transonic small disturbance potential equation shows that the latter is a valid approximation only for flows with shocks that make small angles to the free-stream direction. The wing study presented in the parts II, III, and IV of this report applies to just this case, so the classical transonic equation was used for all the calculations presented herein. However, part I includes the development of a new small disturbance equation for more general cases when the oblique shock angle is greater than, say, 15°.

Parts II, III, and IV cover the application of the numerical method to a practical case – that of the C-141 airplane wing. The C-141 wing was chosen for two reasons. First, it provides a good test for any three-dimensional numerical simulation since it has the complicating features of sweep, taper, camber, and twist; and second, a variety of wind tunnel and flight data are available for comparison with computed results. Part II provides a description of the wing geometry and a discussion of the experimental data emphasizing the influence of viscosity. The numerical method is briefly discussed in part III, and the results are interpreted in part IV.

PART I. DISCUSSION OF BASIC EQUATIONS

Forms of the Potential Equations

The exact nonlinear equation for inviscid, isentropic, two-dimensional potential flow can be written in cartesian coordinates in the form

$$(a^2 - \Phi_x{}^2)\Phi_{xx} - 2\Phi_x\Phi_y\Phi_{xy} + (a^2 - \Phi_y{}^2)\Phi_{yy} = 0 \tag{1a}$$

where a is the local speed of sound, and Φ is the total velocity potential. In terms of total velocity components, this equation becomes

$$\begin{aligned}(a^2 - U^2)U_x &= 2UVU_y - (a^2 - V^2)V_y \\ V_x &= U_y\end{aligned} \tag{1b}$$

The expression of these equations in terms of perturbation potential and velocity components is treated in standard textbooks on fluid flow (see, e.g., ref. 7, p. 204). We will consider two of these perturbation forms in some detail. One form is referred to as the small perturbation equation and is derived by neglecting all terms containing products of perturbation velocity components. This leads to

$$[1 - M_\infty^2 - (\gamma + 1)M_\infty^2 \phi_x]\phi_{xx} - 2M_\infty^2 \phi_y \phi_{xy} + [1 - (\gamma - 1)M_\infty^2 \phi_x]\phi_{yy} = 0 \tag{2a}$$

or

$$[1 - M_\infty^2 - (\gamma + 1)u]u_x = 2M_\infty^2 v u_y - [1 - (\gamma - 1)M_\infty^2 u]v_y$$
$$v_x = u_y \tag{2b}$$

The second form is referred to as the classical transonic equation and is derived from equations (2) by considering the special behavior of fluid flow when the local velocity is close to the speed of sound. It can be expressed as

$$[1 - M_\infty^2 - (\gamma + 1)M_\infty^2 \phi_x]\phi_{xx} + \phi_{yy} = 0 \tag{3a}$$

or

$$[1 - M_\infty^2 - (\gamma + 1)M_\infty^2 u]u_x = -v_y$$
$$v_x = u_y \tag{3b}$$

In equations (2) and (3), the perturbation velocities are defined by

$$U/U_\infty = 1 + u, \quad V/U_\infty = v \tag{4}$$

and the perturbation potential is defined such that

$$u = \phi_x \ , \quad v = \phi_y \tag{5}$$

In the following we will analyze these equations with regard to how they model characteristic lines, sub and supercritical flows, and shock waves.

Characteristics Consistently Ordered With Respect to Perturbation Velocities

When equations (1) through (3) are used to model supersonic flows, they can be analyzed to find characteristic lines; that is, lines across which velocity gradients can be discontinuous. By dividing equations (1b) through (3b) into right- and left-hand sides, we imply that the right side can be evaluated along a given y coordinate, and the result can be used to integrate, or advance a solution in the x direction. One simple way to derive the equation for a characteristic line is to rotate the coordinates through some angle θ_C, as in sketch (a), and ask if there is a value of θ_C for which an advance along ξ is not possible. The result of such a rotation for equation (1b) can be written:

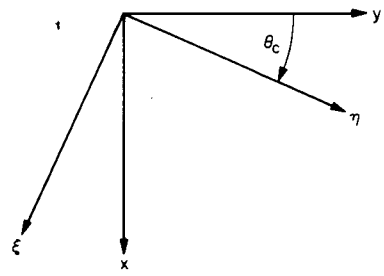

Sketch (a)

$$[A]\begin{bmatrix} U_\xi \\ \\ V_\xi \end{bmatrix} = [B]\begin{bmatrix} U_\eta \\ \\ V_\eta \end{bmatrix} \tag{6}$$

and the advance in ξ is not possible when the matrix $[A]$ is singular; that is, when the determinant of $[A]$ is zero. From this it is well known and easy to show that a characteristic line occurs in solutions to equations (1b) when

$$det[A] = a^2 - (U\cos\theta_C - V\sin\theta_C)^2 = 0 \tag{7}$$

Since in isentropic flow

$$a^2/U_\infty{}^2 = (1/M_\infty{}^2) - [(\gamma-1)/2](2u + u^2 + v^2) \tag{8}$$

equation (7) reduces to the form

$$[(1/M_\infty{}^2) - \cos^2\theta_C] + [2v\cos\theta_C\sin\theta_C - u(\gamma - 1 + 2\cos^2\theta_C]$$

$$-[(\gamma-1)(u^2+v^2)/2 + (u\cos\theta_C - v\sin\theta_C)^2] = 0 \tag{9}$$

where the brackets separate, consecutively, terms having zero-, first-, and second-order powers of the perturbation velocity components.

By an analysis identical to the one just outlined, one can show that the characteristic lines of equations (2) and (3) are

$$(1/M_\infty{}^2) - \cos^2\theta_C + 2v\cos\theta_C\sin\theta_C - u(\gamma - 1 + 2\cos^2\theta_C) = 0 \tag{10}$$

and

$$(1/M_\infty^2) - \cos^2 \theta_c - u(\gamma + 1)\cos^2 \theta_c = 0 \tag{11}$$

respectively. Notice that equations (9) and (10) are identical for both the zero and first powers of the perturbation velocities. In view of their derivation, this is not a surprising result and serves, at this point, only as a check in consistency. Clearly, however, equation (11) is not in agreement with equation (9), even through the first order in the perturbation velocities. Since, to the first-order, oblique shock waves bisect characteristic lines of the same family, this result can influence our choice of equations when we seek to compute flow fields with oblique shocks.

We must proceed with caution, however, since equation (1) itself is based on the isentropic assumption, which precludes, in the strictest sense, its use in connecting regions between which there is a shock having a change in entropy. (The error is quite small for many practical cases, being proportional to the third order of the flow deflection across the shock. Equation (1) and equations derived from it are often used to analyze transonic flows.) Nevertheless, a straightforward way to examine the approximation of a Rankine-Hugoniot shock that can be expected from the use of a given differential equation is found in the examination of the equation's weak solution. This is presented in a following section after some preparatory discussion regarding critical flow and sweep theory.

The Critical Velocity and the Change in Equation Type

If we express a second-order partial differential equation in the form

$$A\Phi_{xx} + B\Phi_{xy} + C\Phi_{yy} + f(\Phi_x, \Phi_y, \Phi) = 0 \tag{12}$$

it is said to be elliptic or hyperbolic, depending on whether the discriminant $(B^2 - 4AC)$ is negative or positive, and it changes type if the discriminant goes through zero. This occurs for equation (1) when $a^2(Q^2 - a^2)$ goes through zero, where $|Q|$ is the magnitude of the total velocity. This gives the classical result that equation (1) changes type when the local flow speed passes through the speed of sound and is hyperbolic on the supersonic side. It is conventional to refer to this speed as the critical speed and the value of the pressure coefficient

$$C_p = \frac{p - p_\infty}{(\rho_\infty U_\infty^2)/2} \tag{13}$$

at which it occurs, as the critical pressure coefficient or $C_p{}^*$. Figure 1 shows a plot of $C_p{}^*$ vs. M_∞ that applies to solutions of equation (1). The relationship is valid under the assumption that the flow is isentropic along a streamline between the reference Mach number M_∞ and any given point. Also shown in figure 1, is the first-order small perturbation approximation to the critical pressure coefficient ($C_p{}^* \approx -2u^*$). This approximation follows at once by neglecting all terms with products of perturbation velocities in the equation for the pressure coefficient and can be expressed as

$$-2u^* \approx 1 - \left(\frac{q^*}{q_\infty}\right)^2 = \frac{-2}{\gamma + 1}\left(\frac{1}{M_\infty{}^2} - 1\right) \tag{14}$$

It is interesting to find the conditions under which equations (2) and (3) change type. For equation (2a), the discriminant is

$$M^4(\gamma^2 - 1)\phi_x{}^2 - M_\infty{}^2\phi_x[\gamma + 1 + (1 - M_\infty{}^2)(\gamma - 1)] + (1 - M_\infty{}^2) - M_\infty{}^4\phi_y{}^2 = 0 \tag{15}$$

Two roots exist for $(M_\infty{}^2\phi_x)$, and the one of physical interest leads to the expression

$$-2u^* = \frac{-2}{\gamma + 1}\left[\frac{1}{M_\infty{}^2} - 1 - \frac{M_\infty{}^2\phi_y{}^2}{1 - [(\gamma - 1)/(\gamma + 1)](1 - M_\infty{}^2)} + \ldots\right] \tag{16}$$

where the * again indicates the value at which the modeling differential equation changes type. Notice that when the term with $\phi_y{}^2$ and terms of higher order in ϕ_y are neglected, equation (16) reduces identically to equation (14), the small perturbation form of the critical pressure coefficient found from the full isentropic equation. It is simple to show that the expression for $-2u^*$ derived from equation (3a) is also identical to equation (14).

In summary, to the lowest order in perturbation velocities, equations (1), (2), and (3) all change type according to the same relationship among u, γ, and M_∞ as given by equation (14).

Simple Sweep Theory

The underlying basis for using wings with swept leading and trailing edges is generally derived by considering a sheared wing of infinite span and constant section (see, e.g., ref. 8). The principal assumption is that the velocity component parallel to an edge is constant or that the perturbation velocity parallel to an edge is zero. Under these conditions a shock, if it occurs, would also have to be parallel to an edge, and its strength would depend only on the component of velocity normal to the edge. This introduces the possibility of redefining the adjective "critical" in a three-dimensional flow so that it is related to a sweep angle, as in Lock and Bridgewater (ref. 9, p. 150). Bagley (ref. 8, p. 16) has gone so far as to use the term *subcritical flow* to mean shock-free flow, regardless of the local Mach number. In this report the word *critical* designates a locally sonic condition or, as discussed in the preceding section, the *condition at which the governing equation changes type.* However, we respect the need for some notation that encompasses the effect of wing sweep to produce wing sections with shock-free supercritical flow. For this purpose, in studying equation (1) the symbol $C_p{}^*$ is used, as before, to designate the pressure coefficient in an isentropic flow at which the local velocity is sonic (the "conventional" definition); and the symbol $C_p{}^*(\theta)$ is used to designate the pressure coefficient in an isentropic flow at which the component of the total velocity normal to some plane, fixed by θ = constant, is sonic. In the following discussion this plane is vertical and is

related to θ in the manner shown in sketch (b). Note that $C_p{}^*(0) = C_p{}^*$, and any variable with an asterisk superscript is defined according to the same logic.

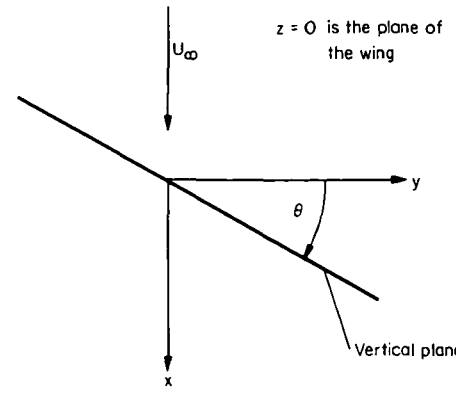

Sketch (b)

Thus, if $q(\theta)$ is the component of velocity normal to an isobar plane, classical sweep theory leads at once to

$$[q^{*2}(\theta) - U_\infty{}^2 \sin^2 \theta] = a^2 \qquad (17)$$

for the critical value of $q(\theta)$. From this one can easily show

$$1 - \left(\frac{q^*(\theta)}{U_\infty}\right)^2 = \frac{-2\cos^2\theta}{\gamma+1}\left(\frac{1}{M_\infty{}^2\cos^2\theta} - 1\right) \qquad (18)$$

Equation (18) can be used to derive $C_p{}^*(\theta)$ without approximation and the result

$$C_p{}^*(\theta) = \frac{2}{\gamma M_\infty{}^2}\left\{\left[\frac{2}{\gamma+1}\left(1 + \frac{\gamma-1}{2} M_\infty{}^2\cos^2\theta\right)\right]^{\gamma/\gamma-1} - 1\right\} \qquad (19)$$

is illustrated in figure 2 for two free-stream Mach numbers. If the small perturbation approximation is applied to equation (18) it simplifies at once to

$$-2u^*(\theta) \approx 1 - \left[\frac{q^*(\theta)}{q_\infty}\right]^2 = \frac{-2\cos^2\theta}{\gamma+1}\left(\frac{1}{M_\infty{}^2\cos^2\theta} - 1\right) \qquad (20)$$

Figure 2 compares equation (19) with equation (20), which is the sweep-theory counterpart of equation (14).

Shocks

So far the discussion has been restricted to properties of genuine solutions[1] to the differential equations – that is, solutions that result in continuous variations in the velocity components. We next inspect the properties of possible weak solutions to these equations. A weak solution can be composed of two genuine solutions separated by a surface across which the dependent variables can be discontinuous. We refer to this surface as a shock, regardless of the form of the hyperbolic equations being investigated. For the Eulerian equations, the jump conditions for the dependent variables

[1] The terms *genuine* and *weak* solutions are used in the sense defined by Lax (ref. 10).

across the shock are referred to as the Rankine-Hugoniot conditions. Different jump conditions prevail for an arbitrary set of hyperbolic partial differential equations. In general, the conditions that must be satisfied across a shock can be found by writing the partial differential equations in conservation law form and connecting the differences in the conserved variables with the direction cosines of the surface across which they are discontinuous (see ref. 10 or 11). Thus if,

$$\partial\vec{E}/\partial x + \partial\vec{F}/\partial y + \partial\vec{G}/\partial z + \vec{H} = 0 \tag{21}$$

is the differential equation,

$$(\Delta\vec{E})\cos\alpha_1 + (\Delta\vec{F})\cos\alpha_2 + (\Delta\vec{G})\cos\alpha_3 = 0 \tag{22}$$

is the equation that must be satisfied across the surface representing the shock. Here Δ signifies the jump of the variable across the shock and $\cos\alpha_1$, $\cos\alpha_2$, and $\cos\alpha_3$ are the direction cosines of the shock with respect to the x, y, and z axes, respectively. The two-dimensional cases are especially simple since for them the shock degenerates to a line. Choose the xy plane; then the local slope of the line is given by

$$\cos\alpha_2/\cos\alpha_1 = -\tan\theta$$

where θ is an angle having the same relation to the y axis as θ_C in sketch (a).

The jump conditions for the isentropic shock embedded in equation (1) are derived and discussed in reference 12. The conditions lead to an implicit relationship for the velocity components on the two sides of the discontinuity, which can be written as

$$G_1 u_1 - G_2 u_2 = (G_1 v_1 - G_2 v_2)\tan\theta \tag{23}$$

where

$$G_i = \left[1 - \frac{\gamma - 1}{2}(u_i^2 + v_i^2)\right]^{1/\gamma - 1}$$

and the subscripts 1 and 2 refer to conditions on the upstream and downstream side of the shock at any given point.

The conservative form of equation (2) can be expressed as

$$\frac{\partial}{\partial x}\left[(1 - M_\infty^2)u - \frac{3-\gamma}{2}M_\infty^2 v^2 - \frac{1}{2}M_\infty^2(\gamma+1)u^2\right] + \frac{\partial}{\partial y}\left[v - M_\infty^2(\gamma-1)uv\right] = 0$$

$$\frac{\partial v}{\partial x} - \frac{\partial u}{\partial y} = 0 \tag{24}$$

and for its jump condition, straightforward algebra leads to the relationship

$$\left[1-\frac{1}{2}M_\infty{}^2(\gamma+1)(u_1+u_2)\right]\tan^2\theta-2M_\infty{}^2(v_2+u_2\tan\theta)+1-M_\infty{}^2-\frac{1}{2}M_\infty{}^2(\gamma+1)(u_1+u_2)=0 \tag{25}$$

The jump condition for equation (3) is important and is derived in some detail. The conservative form is

$$\frac{\partial}{\partial x}\left[(1-M_\infty{}^2)u-\frac{1}{2}M_\infty{}^2(\gamma+1)u^2\right]+\frac{\partial v}{\partial y}=0$$
$$\frac{\partial v}{\partial x}-\frac{\partial u}{\partial y}=0 \tag{26}$$

and the jump conditions first appear in the form

$$(1-M_\infty{}^2)\Delta u-\frac{1}{2}M_\infty{}^2(\gamma+1)\Delta u^2=\Delta v\tan\theta$$

$$\Delta v=-\Delta u\tan\theta$$

Eliminating Δv, and noting that $\Delta u^2=u_1{}^2-u_2{}^2=(u_1+u_2)\Delta u=\bar{u}\,\Delta u$ gives

$$\tan^2\theta=M_\infty{}^2-1+\frac{1}{2}M_\infty{}^2(\gamma+1)\bar{u} \tag{27}$$

or

$$\frac{(-2u_1)+(-2u_2)}{2}\approx\frac{-2}{\gamma+1}\left(\frac{1}{M_\infty{}^2\cos^2\theta}-1\right) \tag{28}$$

This is the condition that must be met across a shock according to the classical transonic theory expressed by equation (3).

Shocks and Supercritical Flow

In the terminology we are using, a simulated flow becomes supercritical when the differential equation changes type from elliptic to hyperbolic. To the lowest order in the perturbation velocities, we have shown that this occurs under the same condition for equations (1) through (3), namely, where

$$-2u=-2u^*\approx\frac{-2}{\gamma+1}\left(\frac{1}{M_\infty{}^2}-1\right) \tag{29}$$

In terms of the definitions and analysis given above, two observations can be made about a simulated flow that has become supercritical:

1. A shock can exist; but, without prescribed boundary conditions, there is nothing that tells us it *must* exist; that is, the simulated flow along a streamline can go supercritical and return to subcritical with or without an intervening shock, regardless of the form of the nonlinear equations being used to model the flow.

2. The critical condition – for example, equation (29) – by itself tells us nothing about the position or intensity of a shock if it does exist. Information about these properties appears in the weak solution of the differential equation and is resolved by a mechanism quite different from that which governs change of type.

Now consider the jump condition for the shock embedded in the equations (24) and (26). Recall that we are considering a three-dimensional, transonic flow having the property that a shock, if it exists, will be nearly vertical, so we need to consider only the effect of θ, its lateral angle of sweep. It is quite possible to study shocks with significant inclination to the free stream in both directions; but, again, the added complexity is unnecessary for our purposes.

When *all* simulated shocks are nearly perpendicular to the free-stream direction so that setting $\theta = v_2 = 0$ is a good approximation, equations (24) and (26) represent the same result. This result applies to the standard two-dimensional studies, of course, and in the form of equation (28) it gives a condition that must be met by the average of the perturbation velocities across the discontinuity. Notice that as u_1 approaches u_2, they both approach u^*. That is, the intensity of a shock perpendicular to the free stream is centered about the critical perturbation velocity, which, in turn, is based on the condition that the equation changes type. For such cases, equations (2) and (3) give essentially the same results, and equation (3) is to be preferred because of its simplicity.

If the boundary conditions are such that a vertical shock is oblique to the free stream, the shock position and intensity could be significantly different depending on whether equation (2) or (3) was used for the simulation. For example, return to equation (25) and consider the special case when $v_2 = -2u \tan \theta$ (sketch (c)), which exists when the component of the perturbation velocity parallel to the shock is zero. That is, the special case when the condition for simple sweep theory applies, and equation (25) reduces to

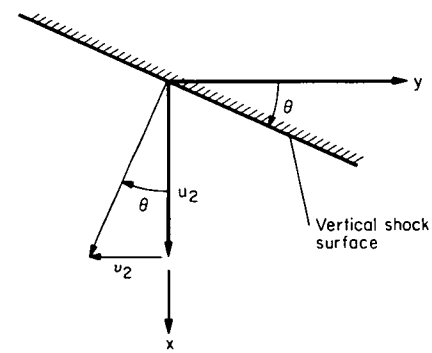

Sketch (c)

$$\frac{(-2u_1) + (-2u_2)}{2} \approx \frac{-2\cos^2\theta}{\gamma + 1}\left(\frac{1}{M_\infty{}^2\cos^2\theta} - 1\right) \tag{30}$$

On the other hand, the jump condition for equation (3), given by equation (28), does not depend on any special relation between u_2 and v_2 and is valid for all values of θ as it stands. Therefore, the

difference between equations (2) and (3) in simulating oblique shocks is apparent from a comparison of equations (30) and (28). This difference is shown in figure 3 for $M_\infty = 0.85$. Shown also is the exact value of $C_p{}^*(\theta)$ for simple sweep theory given by equation (19). Once again, as the strength of the shock vanishes, u_1 approaches u_2, and they both approach a value of $u^*(\theta)$ appropriate for the local conditions. Figure 3 shows that equation (3) is a very poor model for flows with shocks that are more than 30° oblique to the free stream. Equation (2), on the other hand, is acceptable for a wide range of θ, limited only by the accuracy of the small perturbation approximation itself. Hence, for three-dimensional, transonic flows in which the presence of oblique shocks at moderate to large sweep angles is anticipated, the proper form of the transonic small disturbance equation is

$$[1 - M_\infty{}^2 - (\gamma + 1)M_\infty{}^2\phi_x]\phi_{xx} - 2M_\infty{}^2\phi_y\phi_{xy} + [1 - (\gamma - 1)M_\infty{}^2\phi_x]\phi_{yy} + \phi_{zz} = 0 \tag{31}$$

From the above discussion we see that shocks may or may not appear in flow simulations when the differential equations become supercritical. If they do form, they appear as surfaces of discontinuities, the local intensity of which depends on the local surface inclination with respect to the free-stream direction as well as other local and free-stream conditions. We now inspect the effect that these observations have on the interpretation of numerical simulations of transonic flow.

PART II. DESCRIPTION OF THE AIRPLANE WING AND DISCUSSION OF EXPERIMENTAL RESULTS

Several numerical simulations of three-dimensional wings have been reported (refs. 13-15). These studies have included lift and sweep-back but not taper or twist. Further, they were confined to low aspect ratio planforms or biconvex profiles. To test the full capability of a complete wing analysis, we chose to simulate the transonic flow about a wing with a fairly high aspect-ratio planform having twist, sweep, taper, and a blunt, cambered profile. The wing on the C-141 airplane has all of these features; in addition, some flight and wind-tunnel data are available for comparison. Previous studies of a panel model of the C-141 profile (ref. 14) indicated that the calculations are feasible if they can be carried out on an advanced computer such as an IBM 370/195 or a CDC 7600. The numerical procedure and results are presented in part III.

Wing Geometry

The C-141 wing planform is shown in figure 4. It is mounted on top of the fuselage and has a kink in the trailing edge about 43 percent of the span outboard from the root section. Two nacelles are mounted under the wing as shown. The fuselage, kink, and nacelles were not modeled in the calculations. The planform that was modeled is shown by the solid line in figure 5. The actual numbers are shown in figure 5 and result in the following basic parameters:

Sweep (L.E.) = 25.6°

Taper ratio = 0.373

Aspect ratio = 8.0

Thickness ratio = 0.1145

Twist = 5° (linear)

At the time the flow field was calculated, we were not aware that the C-141 profile varied in the span direction. For the computations we assumed that the profile was uniform and used the section coordinates at the span station y/b = 0.389 (given in table 1), which is the measurement station closest to the kink as shown in figure 5.

Brief Review of Viscous Effects on Transonic Flow Experiments

Before proceeding with a discussion of the experimental results, the following remarks should be made. It is very well known that low Reynolds number wind-tunnel tests of the pressure distribution on a complete C-141 model do not agree with flight conditions (see, e.g., ref. 16), a discrepancy that is attributed mostly to differences in viscous scaling rather than wind-tunnel wall or flow effects. The purpose of reference 16 was to present a technique for overcoming this difficulty in wind-tunnel facilities by testing wing panel models with stream-lined end plates to obtain experimental data at much higher Reynolds numbers than are possible for complete models. This is a perfectly acceptable procedure, and its success is indicated by the results presented in reference 16.

One purpose of the present report is to suggest an alternate method for anticipating the loads and pressure distributions on wings at flight conditions. In this method, numerical simulations are performed that, in the absence of boundary-layer interaction, can be said to represent unseparated flows at an infinite Reynolds number.

At the present time the difficulty in predicting the transonic flow that exists in actual flight from either wind-tunnel or computer simulations is generally attributed to a viscous-inviscid coupling of two types of turbulent boundary-layer separations (ref. 17). One of these, called *pressure gradient* or *trailing-edge* separation, is associated with trailing-edge conditions. It can occur at any speed, and depends strongly on Reynolds number. It is connected with the loss of lift that experimental results show relative to theoretical results for the same wing at the same angle of incidence if the theoretical results are based on the enforcement of the Kutta condition in a potential flow calculation. The other type of separation, called *shock-induced* separation, is generally considered to be insensitive to Reynolds number and depends primarily on the pressure jump across the surface of the shock.

In reference 17, it is argued from experimental evidence that shock-induced separation cannot occur until a free interaction compression (just outside the boundary layer) turns the flow through 6.6°. Given sonic conditions on the downstream side of the shock the lowest Mach number on the upstream side meeting this condition is about 1.32. It is further hypothesized that the shock will continue to induce local separation for upstream Mach numbers greater than about 1.32, although the angle of separation will continue to be around 6.6° for the higher Mach numbers. In view of these arguments and examinations of other data, a set of tentative hypotheses (also suggested in ref. 17) has been adopted:

1. As the free-stream Mach number in a transonic two-dimensional flow is increased, a shock will (in general) form and commence to move downstream. The Mach number just ahead of the shock can increase to about 1.2 without danger of shock-induced separation.

2. As the free-stream Mach number is further increased, the shock will move farther downstream and its upstream Mach number may go as high as about 1.4 without shock-induced separation, but this separation might occur anywhere between $1.2 \lesssim M \lesssim 1.4$. The data in figure 6(b), for example, show a break at $M \approx 1.3$, which is presumed to be due to shock-induced separation occurring at Mach numbers higher than this.

3. When the shock does separate the boundary layer, the interaction causes the shock to weaken and move upstream as much as 20 percent of the chord from its unseparated location.

Figure 7 relates the local pressure coefficient to the free-stream Mach number given by the equation

$$C_p = \frac{2}{\gamma M_\infty^2}\left(\left\{\frac{1 + [(\gamma - 1)/2]M_\infty^2}{1 + [(\gamma - 1)/2]M^2}\right\}^{\gamma/\gamma-1} - 1\right)$$

for the range of conditions covered in the three hypotheses just outlined.

In reference 17, it is shown that the two types of separation (trailing edge and shock induced) can amplify one another when they occur together. There appears to be good reason to believe that all variations of these viscous-inviscid interactions appear in the data presented below.

The Experimental Data

Flight and wind-tunnel data for the C-141 airplane and its model are shown in figures 8(a) and (b). The data are taken directly from reference 16, and represent pressure distributions on the upper surfaces of the wings. To inspect these data in light of the various possible separation phenomena discussed above, we first consider the flight data for $M_\infty = 0.825$, $Re = 36 \times 10^6$ shown in figure 8(a). It is expected that some trailing-edge separation exists since this is generally the case for all wings and wing sections in flight or wind tunnels (typically a loss of 10 percent in lift under the conditions reported here). However, there is no indication of shock-induced separation. The pressure coefficient just ahead of the shock is about -1.07 which, according to figure 7, is just within the allowable limits of unseparated flow according to the second hypothesis given in the preceding section. (The complicating factor of sweepback also enters the picture. However, on the basis of the computed results the shock is probably swept no more than 13°.)

When the flight Mach number is increased to 0.85, the local Mach number ahead of the shock is pushed above the "allowable" limit. From the appearance of the data, shock-induced separation occurs causing the shock intensity to decrease and the shock location to be moved upstream from its position in an inviscid flow (about 20 percent of the chord according to calculations presented in the next part). On the other hand, when the Mach number is fixed at 0.825 and the Reynolds number is reduced from 36×10^6 to 8.5×10^6, the data from the model show that the shock also moves

upstream. Presumably, this is attributable to trailing-edge separation, which is strongly influenced by Reynolds number.

Finally, when the Mach number for the model tests is increased to 0.85, the data shown in figure 8(b) can be interpreted to show strongly coupled effects of both types of separation.

PART III. DISCUSSION OF THE NUMERICAL PROCEDURE AND PARAMETERS

The procedure used in the calculations presented in this report is as follows:

1. Test the local flow condition using central differencing.

2. If, on the basis of this test, the flow is supersonic, use upstream differencing for the streamwise derivative.

3. If, on the basis of this test, the flow is subsonic, use central differencing.

This procedure consistently underestimates the strength of the shock and appears to cause its location to fall upstream of its position as determined by the exact solution of the governing partial differential equation. This can easily be shown to be true in the case of a one-dimensional flow equation, and is implied to be true by experience with two- or three-dimensional cases.

On the other hand, the viscous effects brought about by shock-boundary-layer interaction also cause the experimental strength and location of the shock to differ from those values predicted on the basis of a theory that neglects viscosity. If the predominant viscous effect is limited to trailing-edge separation, then it appears by coincidence that computed flows (using methods based essentially on the procedure described above) and experimental flows are in good agreement. A substantiation of this remark can be found by comparing the computed results for two-dimensional flows shown in figure 6(a) with the high Reynolds number experimental results shown in figure 6(b). The usefulness of this fortuitous circumstance cannot be overlooked now that it has been established by such a wide variety of comparisons between calculated and experimental results. It is hardly a satisfactory state of affairs, however, and further work is required to develop methods that account for viscosity in a rational manner.

Further details of the numerical method used to simulate the flow are described in references 14 and 15. On the basis of experience gained in these calculations, the authors are developing methods having greater efficiency and reliability than that given in references 14 and 15.

Part of the numerical technique was to use a coordinate transformation that transformed the wing into a rectangular area for the final mesh that was used in the differencing. Both a coarse (~80,000 points) and a moderately fine (~200,000 points) mesh were used for the calculations; the results are described in the next part. In both cases the chord distribution of points was clustered near the leading and trailing edge, and nearly equally spaced over the remaining portion of the wing. As the mesh receded from the wing, the intervals between points were successively increased in all directions. The actual array of (x, y, z) points used was (68, 23, 49) for the coarse mesh and (82, 49, 49) for the finer one. Other details of the calculations are:

	$\Delta x/c$ Leading Edge	$\Delta x/c$ Elsewhere on Wing	$\Delta y/b$ on Wing	Seconds/Iteration IBM 370/195
Coarse mesh	0.0025	0.05	~0.06	1.3
Fine mesh	.0025	.025	.025	7.0

PART IV. INTERPRETATION OF NUMERICAL SIMULATIONS AND COMPARISON WITH EXPERIMENTAL RESULTS

All calculations presented were based on the equation

$$[1 - M_\infty^2 - (\gamma + 1)M_\infty^2 \phi_x]\phi_{xx} + \phi_{yy} + \phi_{zz} = 0 \tag{32}$$

The Kutta condition was applied at the trailing edge by requiring that the pressure be continuous across the wake. The vortex sheet was fixed in the plane of the wing, and its spanwise strength was proportional to the span loading. The boundary conditions were applied by specifying the upper and lower vertical velocities above and below a horizontal plane according to the local thickness, camber, and angle of attack of the wing surface (thin-airfoil boundary conditions; see ref. 14 for details). In studies of two-dimensional profiles, this approach has been found to give results that compare reasonably well with data for airfoil nose shapes similar to that found on the C-141 section (those having "nonpeaky" pressure distributions, see ref. 18). One would expect the approach to give comparable results in three-dimensional studies having twist, taper, and sweep, except for cases in which oblique shocks form on surfaces at an angle greater than about 15° with the free stream. The latter restriction is brought about by the use of equation (32), rather than the boundary condition approximation, and follows from the discussion given in part I of this report.

It is of fundamental interest to study the numerical resolution of shocks that are admitted by equation (32), whether or not they represent a valid approximation of normal or oblique Rankine-Hugonoit shocks. As noted in part I, the interpretation of a shock is related entirely to an analysis of the set of differential equations and boundary conditions from which it was derived and is valid and applicable to that set irrespective of how that set models a physical process. Therefore, in spite of the fact that some of the following numerical results for the $M_\infty = 0.853$ case may have no quantitative physical counterpart, their qualitative analysis is quite instructive.

Examples of Normal and Oblique Shocks, $M_\infty = 0.853$

The calculations made for $M = 0.853$ were carried out on a relatively coarse mesh (80,000 points) and are presented in figures 9, 10, and 11. The computed shock location at the span location $y/b = 0.414$ occurred at $x/c \approx 0.78$. This fact, taken in conjunction with the results shown in

figure 8, is the basis for our conclusion that the flight test results for $M = 0.853$ are strongly affected by shock-induced separation. However, they are still worth considering from an instructional point-of-view.

Figure 9 presents the computed results for the pressure on the upper and lower surface of the wing at the root section. Notice that the curve for the pressure on the upper surface shows four places where there are sudden changes in curvature. To properly interpret the solution, one must decide whether these are valid representations of an analytic solution to equation (32) or invalid representations caused by an inadequate numerical approximation. Then, if they are considered to be valid, one must decide whether they represent an ordinary and continuous response to local wing shape, or a weak solution with a shock.

Seeking out the possibility of a shock at the root section, we note that (1) a shock can occur at any position where C_p ($= -2u$) is greater than 0.312 (where eq. (32) changes type); (2) because of symmetry, at this station it cannot be oblique to the y axis; and (3) because of (1) and (2), the average C_p across any discontinuity must also be 0.312. With this in mind, we find that figure 9 shows two locations where the results could be associated with a shock, one at $x/c = 0.170$, and the other at 0.945. Before considering these results in detail, let us examine similar phenomena further down the wing span.

Figure 10 presents pressure distributions at three consecutive mesh intervals centered at the $y = 0.623$ station, and figure 11 presents a computed isobar pattern for the upper surface of the wing central portion. Every span station used for a mesh plane is identified, thus indicating the coarseness of the mesh spacing in the span direction.

Considering first the sudden pressure jump on the aft portion of the upper surface in figures 9 and 10. In view of the consistency of this behavior along the entire wing span, it is reasonable to regard this as a numerical representation of a rather strong shock. The isobar pattern indicates that the discontinuity occurs along a surface inclined about 13° to the free stream. At $M = 0.853$, $C_p{}^*(13°) \approx 0.373$; the dashed lines in the figures represent our estimate of the actual shock approximated by the numerical calculations. The sharp cusp extending into the positive pressure coefficient area represents our estimate of a local logarithmic singularity in the streamwise gradient of the velocity, which should appear in the solution but which is not well resolved in these calculations (ref. 19).

Consider next the pressure distributions on the upper surface near the wing leading edge in figure 10. The curve representing the solution at $y/b = 0.623$ shows a pronounced dip at $x/c \approx 0.15$, but the curves at mesh stations on either side show little or no such tendency. Comparisons of successive runs showed that the solution in this region was not stationary; that is, the loop in the isobars near the leading edge of station 0.623 shown in figure 11 had a spanwise fluctuation with iteration count. This can occur in "converged" solutions to difference equations when, for example, some of the eigenvalues of the algebraic equations are complex and have absolute values equal to one.[2] We hypothesize that this situation has occurred here and attribute it to the coarseness of the mesh. This aspect of the interpretation will be raised again in the discussion of the $M_\infty = 0.825$ solution.

---

[2]The solutions are converged in the sense that further iteration will not significantly reduce the effect on the solution of those eigenvalues with modules less than one.

The important point to be raised regarding the leading-edge pressure behavior presented in figures 9 and 10 is that the abrupt changes at $x/c = 0.15$ *could* be attributed to an attempt by the numerical procedure to form a shock at this location. At this point, it is impossible to say that a converged stationary solution based on a finer mesh would exhibit the same result. However, the calculations indicate the strong possibility that wings of the type being studied may have weak oblique leading-edge shocks preceding much stronger ones that are nearly normal to the free stream.

Comparison of Numerical Simulations and Experiments for $M_\infty = 0.825$

A set of calculated pressure distributions for the upper and lower surfaces of the C–141 wing flying at $M_\infty = 0.825$ is shown in figure 12. (The Kutta condition at the trailing edge was satisfied by making the upper and lower pressures join at the first point not shown in the figures.) Every fourth spanwise station of the moderately fine (200,000 points) mesh calculation is presented. Figure 13(a) and (b) show upper surface isobar plots constructed from the coarse and fine mesh computations, respectively. For completeness, figure 14 includes the span load distribution obtained from the computed circulation for the fine mesh. At two points, the circulation was also calculated from a numerical integration of the chord loading. The two methods give the same value within the accuracy to which one can estimate the shock location.

It is appropriate to consider the accuracy of these calculations insofar as they represent a solution to equation (32). We can discuss the effect of mesh refinement, the degree of convergence and the resolution of the singularity at the shock-wing juncture.

The general effect of going from an 80,000-point to a 200,000-point mesh is demonstrated by comparing (a) and (b) of figure 13. The isobar patterns are significantly smoother for the finer mesh. A more detailed visualization is given in figure 15, where section pressure distributions are shown for both mesh sizes at $y/b \approx 0.4$. The better resolution of the peak pressure and shock position for the fine mesh calculations is evident.

The criterion for calling a solution converged in a nonlinear relaxation procedure is not simple. It is usually based on the iterative history of certain residuals and is generally considered acceptable only when the final result is stationary. In our calculations the deciding parameters were the residuals of the span circulation, and we accept the less stringent criterion for convergence given in the preceding footnote. Under this condition two successive "converged" solutions for the coarse mesh are shown in figure 16(a). On the lower surface, both solutions were the same; hence only the upper surface is shown. Figure 16(b) shows two successive "converged" solutions for the finer mesh. Completely stationary convergence is not indicated in either case, although experience with studies of two-dimensional flows suggests that the solution found by the finer mesh has settled down to the place where the shock location is correctly located to within about one chordwise mesh point, or 2.5 percent chord for the fine mesh.

Some final results showing a comparison of flight, wind tunnel, and computed data on the upper surface of the C–141 wing are shown in figure 17. The calculations were carried out for an airplane flying at 0° angle of attack; that is, for a linearly twisted wing inclined +4° to the free stream at the root, and −1° to the free stream at the tip sections. No attempt was made to match flight angle of attack, since such a comparison is invalidated by trailing-edge viscous effects. Parameters that matched fairly well were leading-edge pressure gradient, peak pressure coefficient, and integrated

upper surface loading. The discrepancy in pressure curvature in the region $0.1 \leqslant x/c \leqslant 0.4$ is not understood. The diference in shock location given by flight and numerical simulation is within the range to be expected on the basis of two-dimensional experience.

After comparisons were made with the data presented in reference 16, some additional flight data on the upper and lower surfaces of the wing and at different span locations were obtained. These data are shown in figures 18 and 19 together with the numerical results already discussed. Note that the upper surface comparison for $M_\infty \approx 0.82$ and $y/b \approx 0.2$ and 0.4 in figure 18(a) and (b) are quite good, while the lower surface agreement is quite poor. This is to be expected because of the body and nacelle interference on the lower surface at these inboard stations. (It should be mentioned that the wing is mounted on top of the fuselage.) The upper surface pressure coefficients shown in figure 18 indicate that the in-flight shock sweep is greater than that of the computed shock. This is understandable because the airplane wing section is varied in the span direction to sweep the shock thereby decreasing its strength. In the calculation this span variation of wing section was neglected.

CONCLUSIONS

Calculations were performed that numerically simulated the three-dimensional, transonic ($M_\infty = 0.825$) flow field about the C-141 airplane wing. Computed results compared favorably with flight data for cases in which the flow was not separated by embedded shock waves. In fact, the computed results predicted the in-flight ($Re = 36 \times 10^6$) pressure distribution more accurately than the wind-tunnel tests ($Re = 8.5 \times 10^6$), which showed appreciable trailing-edge separation. Results indicate that the inviscid, computational method can be usefully applied to analyze three-dimensional transonic flows of engineering interest. The numerical algorithm is currently being extended to treat flows with shocks that are more oblique and geometries that include simple wing-body combinations.

Ames Research Center
National Aeronautics and Space Administration
Moffett Field, Calif., 94035, May 21, 1973

REFERENCES

1. Magnus, R.; and Yoshihara, H.: Steady Inviscid Transonic Flows Over Planar Airfoils: A Search for a Simplified Procedure. NASA CR 2186, 1972.

2. Murman, E. M.; and Cole, J. D.: Calculation of Plane Steady Transonic Flows. AIAA J., vol. 9, no. 1, Jan. 1971, pp. 114-121.

3. Steger, J. L.; and Lomax, H.: Generalized Relaxation Methods Applied to Problems in Transonic Flow. Lecture Notes in Physics, vol. 8. Proceedings of the Second Intl. Conf. on Numerical Methods in Fluid Dynamics, Berkeley, Sept. 15-19, 1970 (M. Holt, ed.), Springer-Verlag, 1971, pp. 193-198.

4. Garabedian, P.; and Korn, D.: Analysis of Transonic Airfoils. Comm. P. & Appl. Math., vol. XXIV, 1971.

5. Jameson, A.: Transonic Flow Calculations for Airfoils and Bodies of Revolution. Grumman Rep. 390-71-1, 1971.

6. Yoshihara, H.: A Survey of Computational Methods for 2D and 3D Transonic Flows With Shocks. Lecture Notes for AGARD-VKI Lecture Series 64, "Progress in Numerical Fluid Dynamics," 5-9 March 1973.

7. Liepmann, H. W.; and Roshko, A.: Elements of Gas Dynamics. John Wiley and Sons, Inc., New York, 1967.

8. Bagley, J. A.: Some Aerodynamic Principles for the Design of Swept Wings. Progress in Aeronautical Sci., vol. 3 (Ferri, Kuchemann, and Sterne, eds.), Pergamon Press, New York, 1962.

9. Lock, R. C.; and Bridgewater, J.: Theory of Aerodynamic Design for Swept-Winged Aircraft at Transonic and Supersonic Speeds. Progress in Aeronautical Sci., vol. 8 (D. Kuchemann, ed.), Pergamon Press, Oxford, 1967.

10. Lax, Peter D.: Weak Solutions of Nonlinear Hyperbolic Equations and Their Numerical Computation. Communications of Pure and Applied Mathematics, vol. 7, no. 1, Feb. 1954, pp. 159-193.

11. Lomax, Harvard; Kutler, Paul; and Fuller, Franklin B.: The Numerical Solution of Partial Differential Equations Governing Convection. AGARDograph 146, AGARD-AG-146-70, 1970.

12. Steger, Joseph L.; and Baldwin, Barrett S.: Shock Waves and Drag in the Numerical Calculation of Isentropic Transonic Flow. NASA TN D-6997, 1972.

13. Bailey, Frank R.; and Steger, Joseph L.: Relaxation Techniques for Three-Dimensional Transonic Flow About Wings. AIAA Paper 72-189, Jan. 1972.

14. Ballhaus, William F.; and Bailey, Frank R.: Numerical Calculation of Transonic Flow About Swept Wings. AIAA Paper 72-677, June 1972.

15. Bailey, Frank R.; and Ballhaus, William F.: Relaxation Methods for Transonic Flow About Wing-Cylinder Combinations and Lifting Swept Wings. Lecture Notes in Physics, vol. 19. Proceedings of the Third Intl. Conf. on Numerical Methods in Fluid Dynamics, Paris, France, July 3-7, 1972 (H. Cabannes and R. Temam, eds.), Springer-Verlag.

16. Cahill, Jones F.; Treon, Stuart L.; and Hofstetter, William R.: Feasibility of Testing a Large-Chord, Swept-Panel Model to Determine Wing Shock Location at Flight Reynolds Number. AGARD Proc. 83, Paper 17, April 1971.

17. Alber, E. E.; Bacon, J. W.; Masson, B. S.; and Collins, D. J.: An Experimental Investigation of Turbulent Viscous-Inviscid Interactions. AIAA Paper 71-565, June 1971.

18. Krupp, J. A.; and Murman, E. M.: The Numerical Calculation of Steady Transonic Flows Past Thin Lifting Airfoils and Slender Bodies. AIAA Paper 71-566, June 1971.

19. Zierep, J.: Der senkrechte Verdichtungsstoss am Gekrümmten Profil. ZAMP, vol. IXb, 2958, pp. 764-776.

TABLE 1.– C-141 WING SECTION COORDINATES (STREAMWISE)

[y/b = 0.389]

Upper Surface		Lower Surface	
x/c	z/c	x/c	z/c
0.0003	0.0042	0.0005	-0.0029
.0008	.0059	.0009	-.0041
.0013	.0073	.0017	-.0058
.0018	.0084	.0031	-.0080
.0053	.0131	.0059	-.0109
.0076	.0154	.0099	-.0141
.0112	.0182	.0165	-.0178
.0160	.0213	.0217	-.0201
.0233	.0252	.0373	-.0250
.0480	.0343	.0681	-.0311
.0728	.0408	.0936	-.0345
.0978	.0458	.1038	-.0356
.1178	.0492	.1242	-.0375
.1478	.0534	.1547	-.0398
.1979	.0589	.1750	-.0410
.2480	.0630	.2053	-.0424
.2980	.0659	.2557	-.0441
.3480	.0678	.3059	-.0451
.3979	.0688	.3560	-.0453
.4477	.0688	.4058	-.0449
.4974	.0678	.4554	-.0438
.5470	.0659	.5048	-.0421
.5965	.0630	.5541	-.0399
.6461	.0591	.6025	-.0369
.6962	.0543	.6521	-.0334
.7465	.0485	.6845	-.0307
.7967	.0414	.7247	-.0278
.8472	.0329	.7846	-.0225
.8976	.0235	.8341	-.0180
.9986	.0017	.8670	-.0148
		.8999	-.0114
		.9164	-.0096
		.9651	-.0039
		.9822	-.0019

Page Intentionally Left Blank

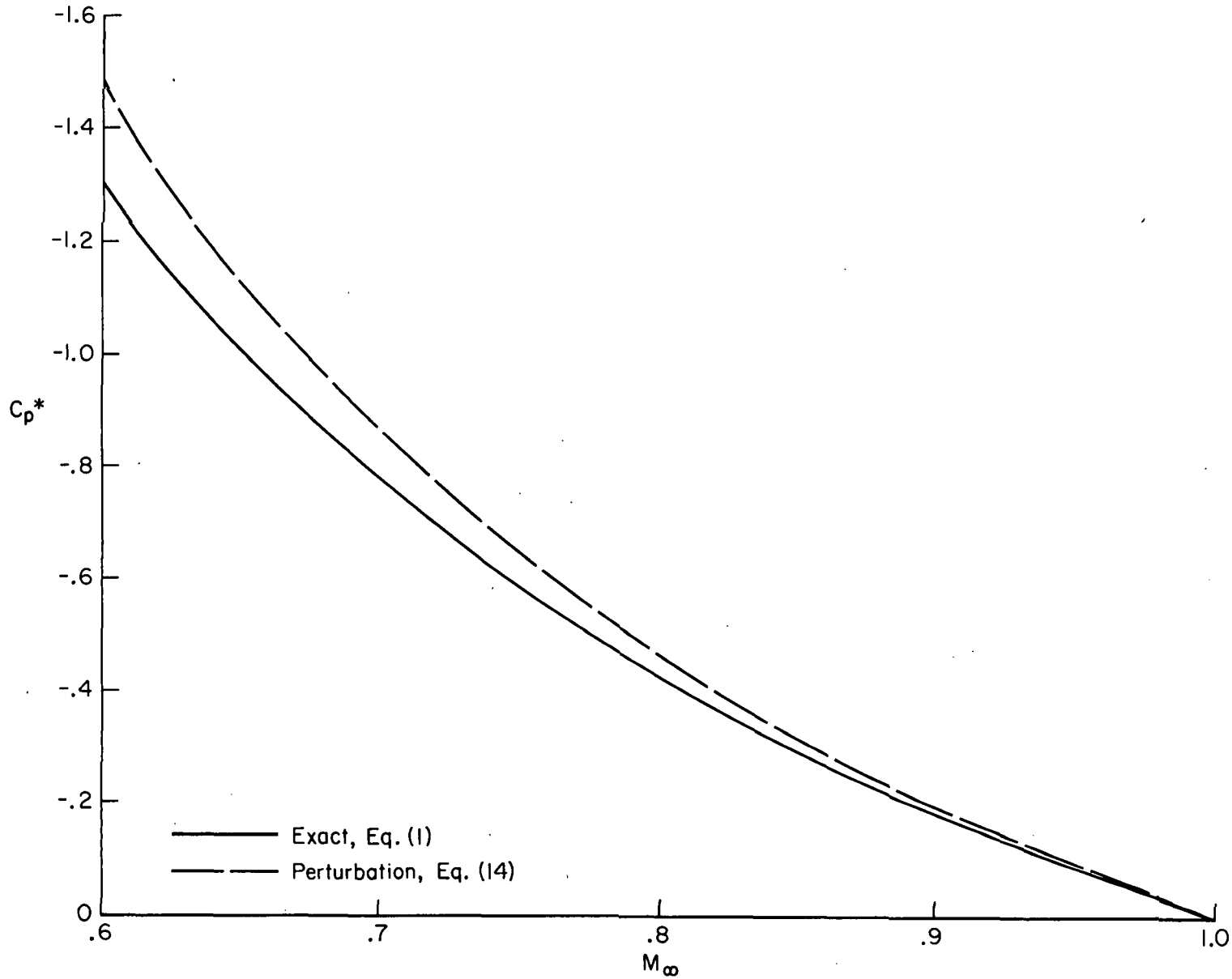

Figure 1.– Critical pressure coefficient vs. free-stream Mach number given by Eqs. (1) and (14).

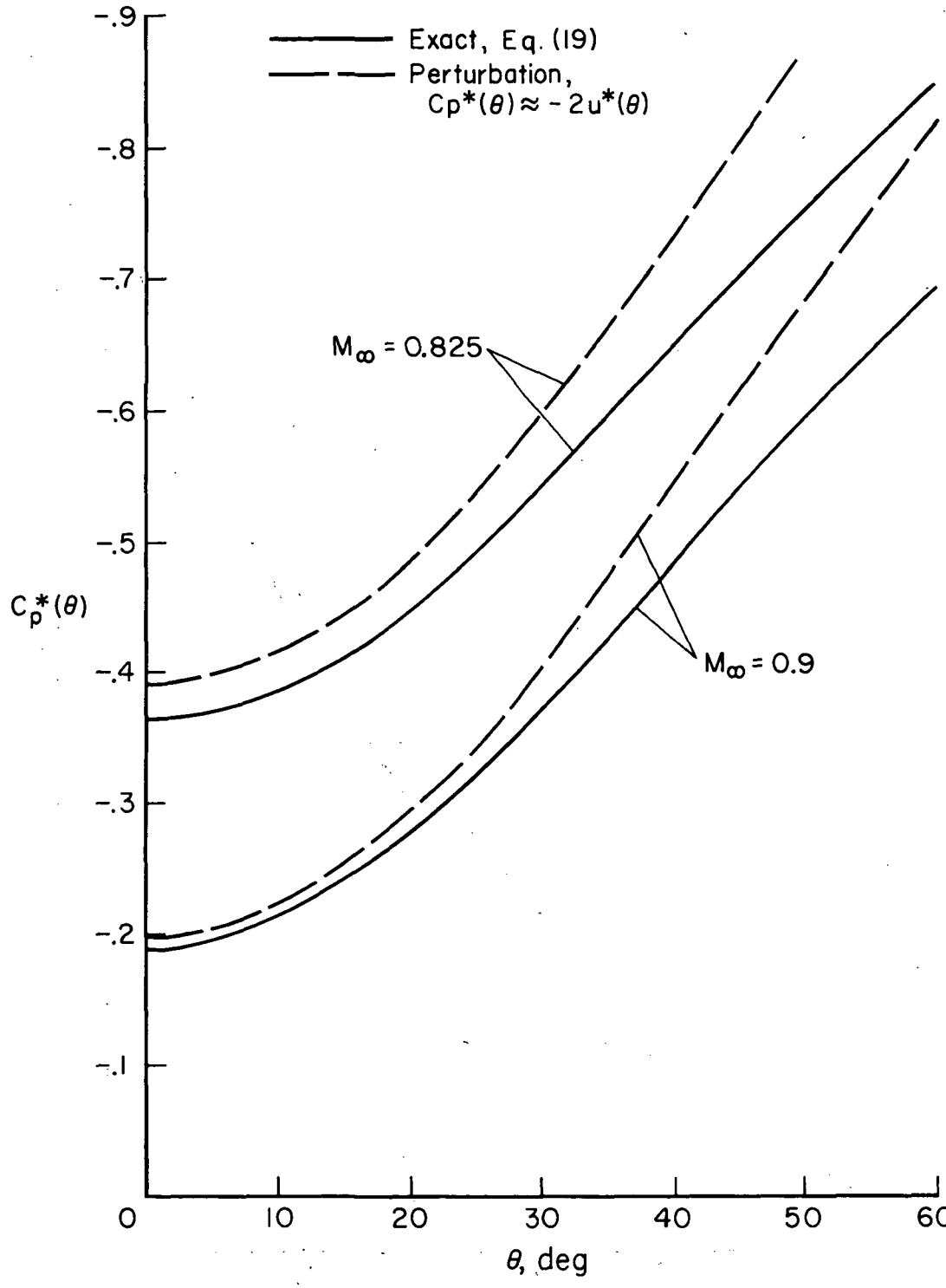

Figure 2.– Approximations to $C_p^*(\theta)$ vs. θ given by Eqs. (19) and (20).

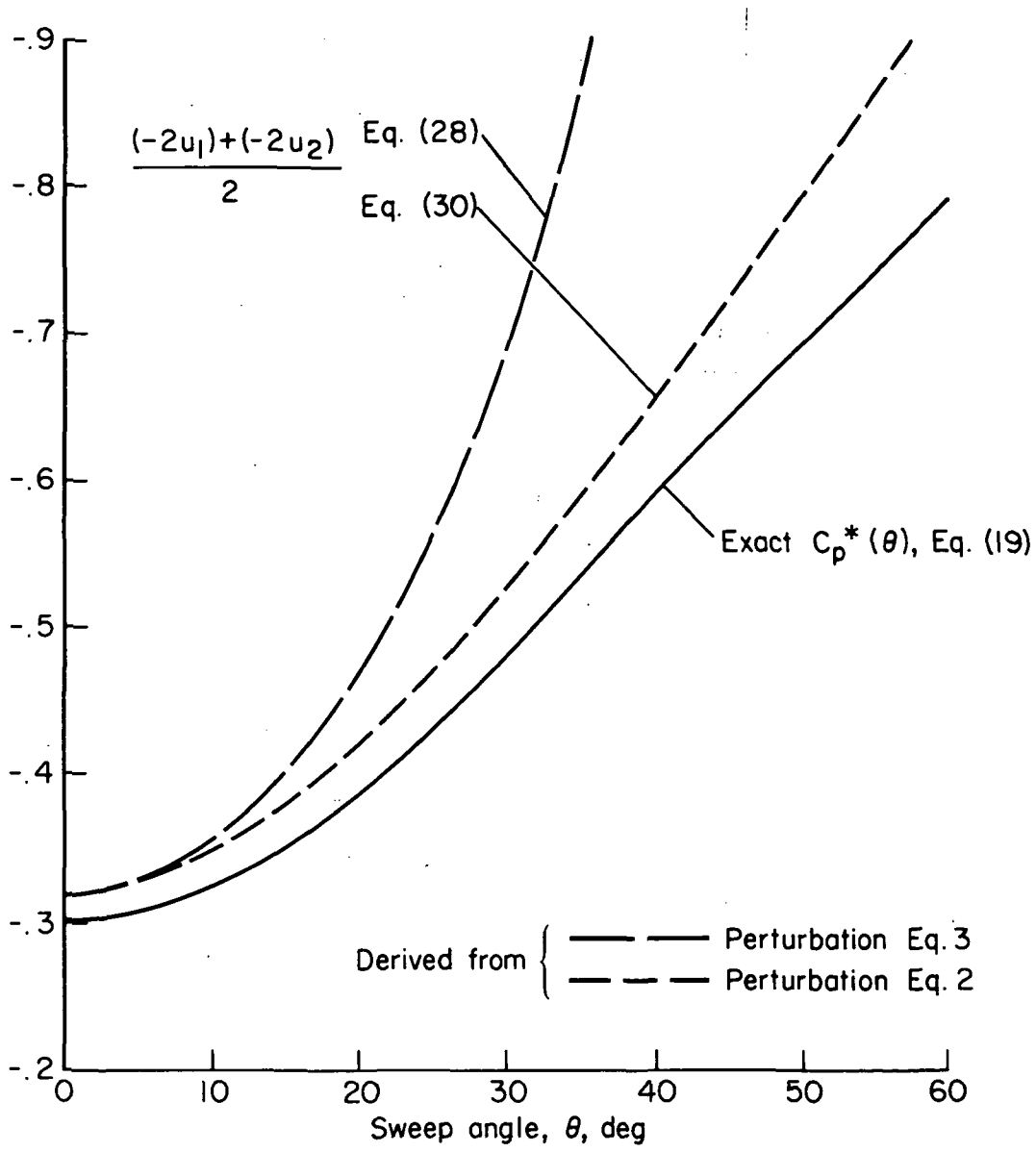

Figure 3.– Exact and approximate values of $C_p^*(\theta)$ for $M_\infty = 0.85$.

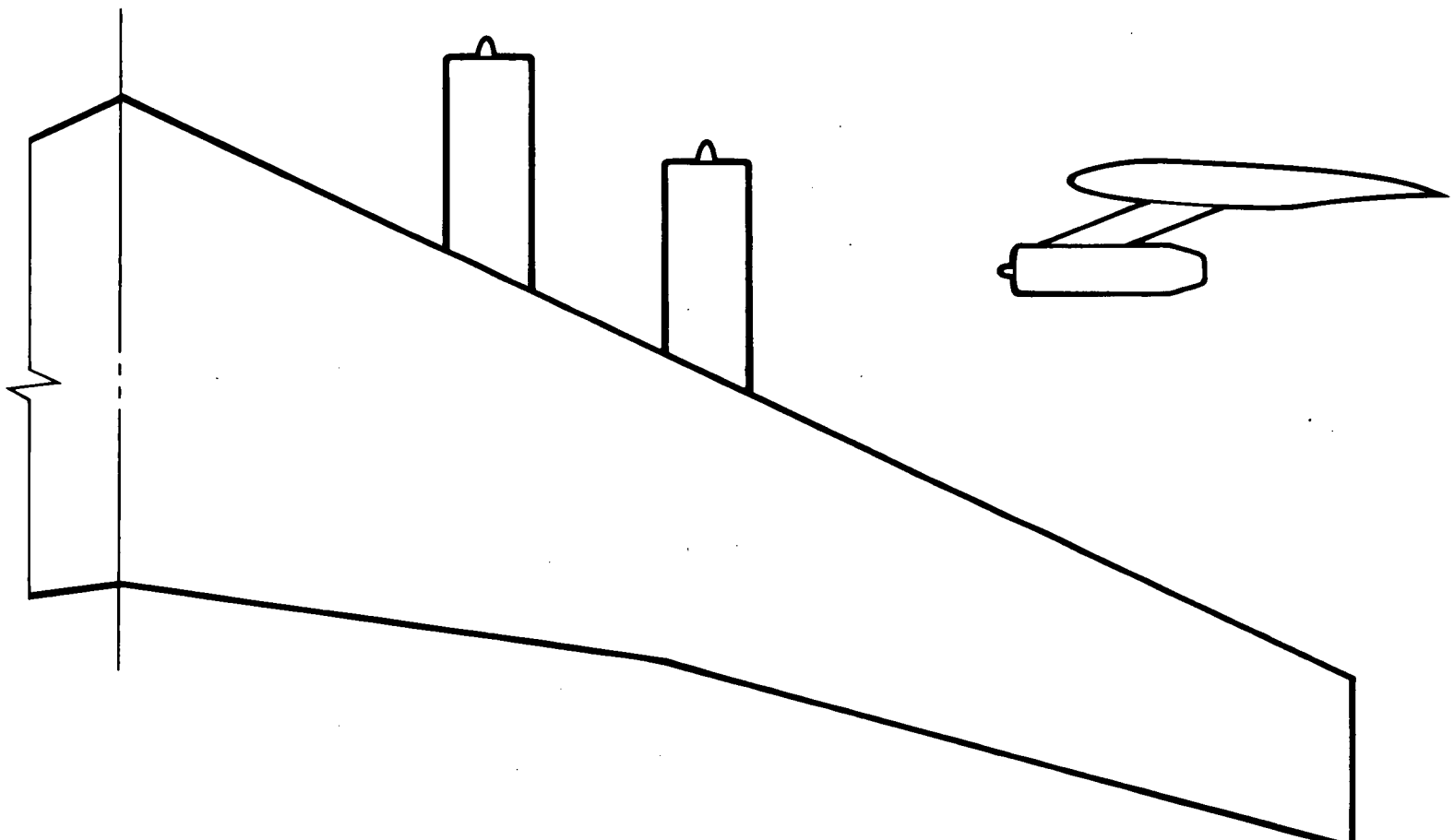

Figure 4.– Shape of C-141 wing planform together with nacelle locations.

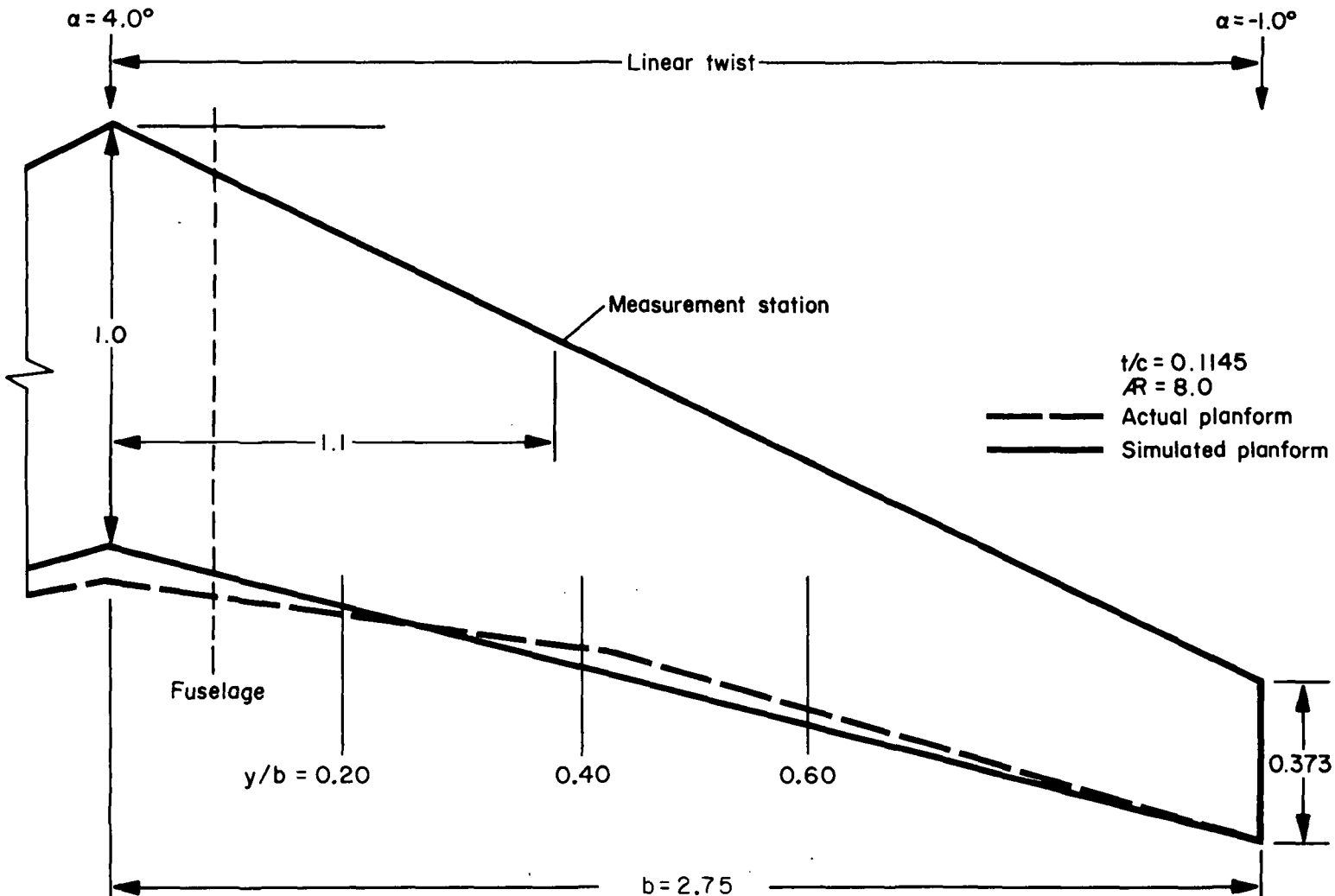

Figure 5.– Comparison of actual and simulated C-141 wing planform.

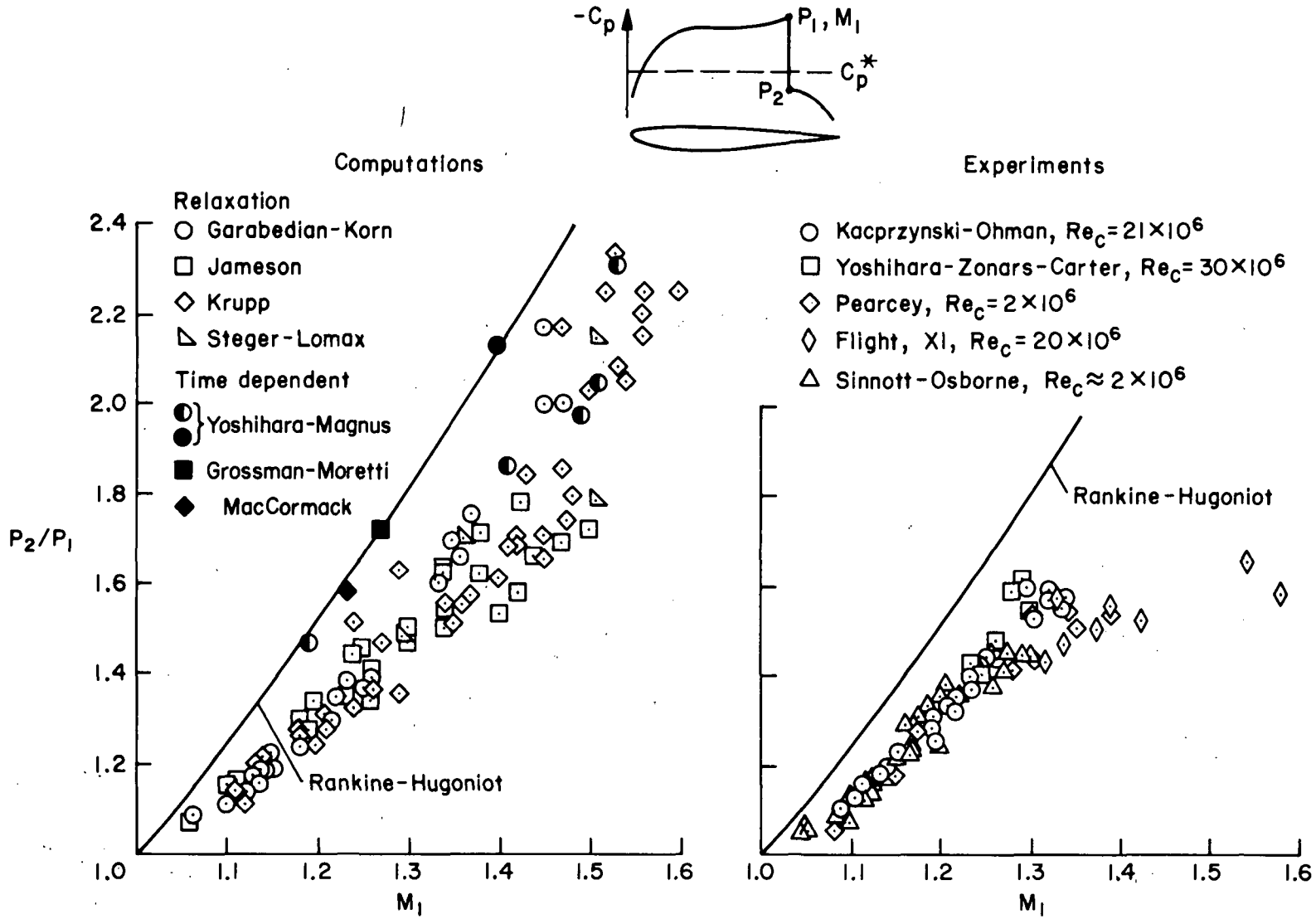

(a) Computed.

(b) Experimental.

Figure 6.– Shock-wave pressure jump on airfoils in transonic flow.

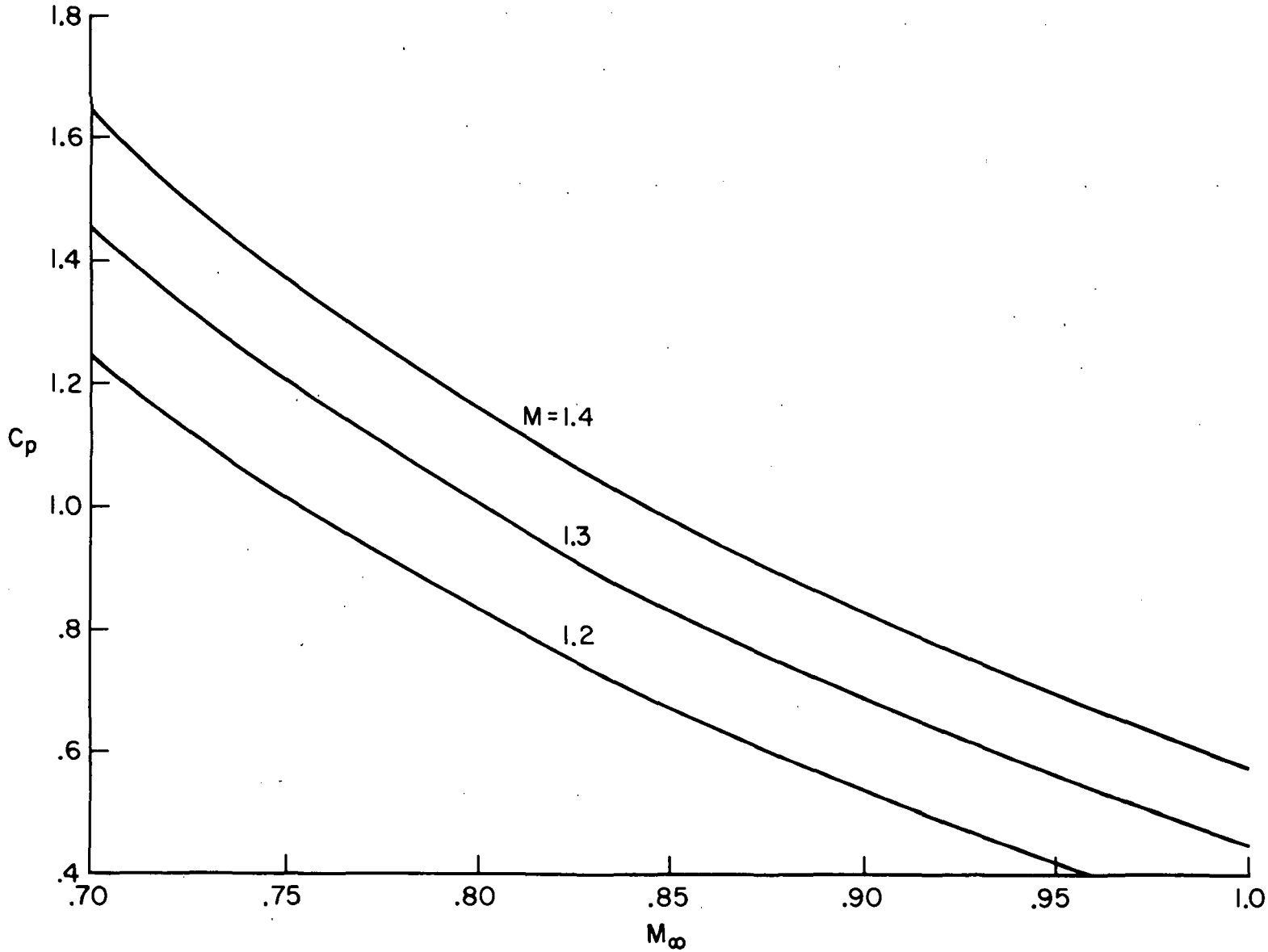

Figure 7.– Relation between local pressure coefficient and Mach number and free-stream Mach number for isentropic flow.

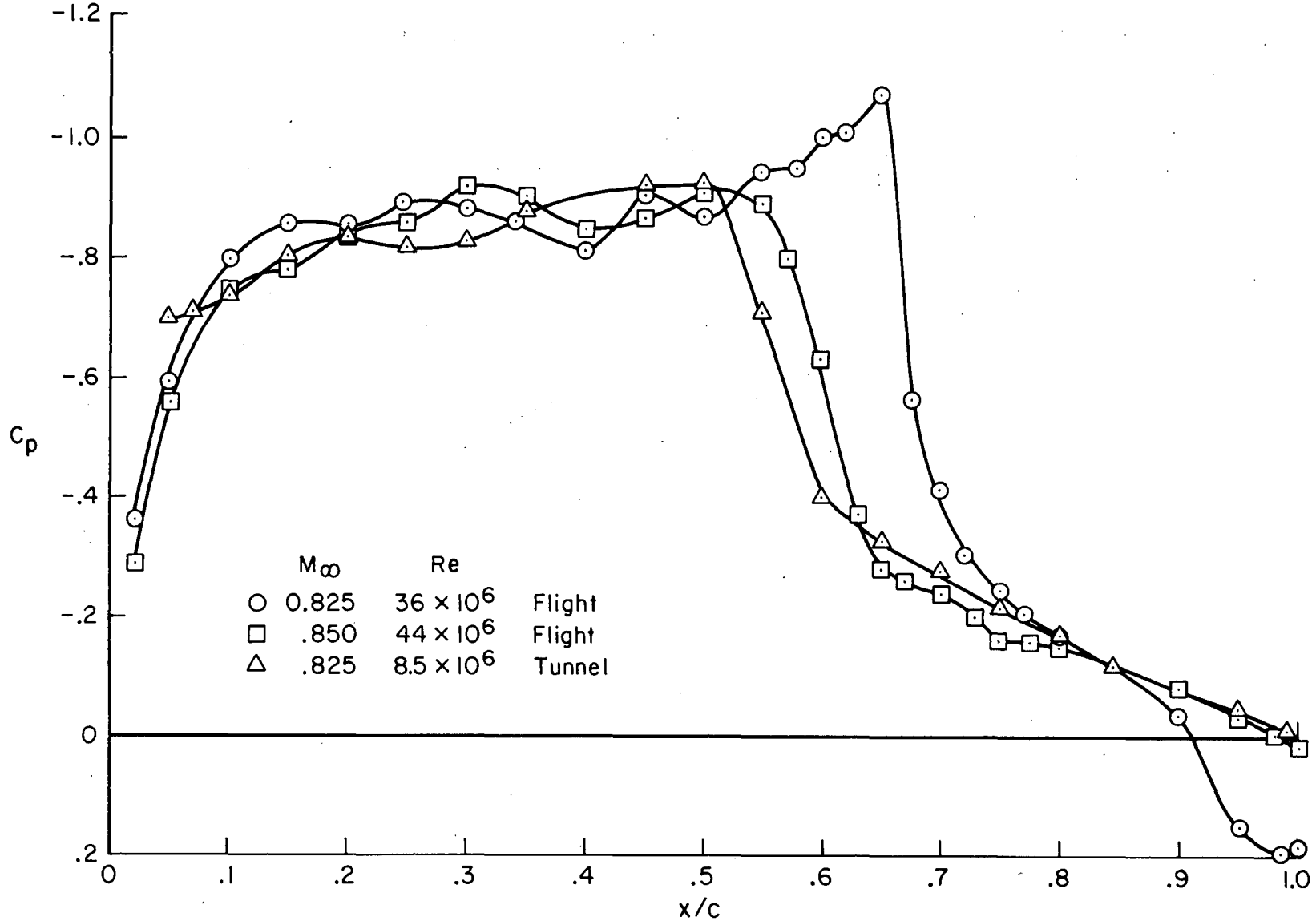

(a) Flight and tunnel, $M_\infty = 0.825$ and 0.85.

Figure 8.– Flight and wind-tunnel data for C-141 airplane and model.

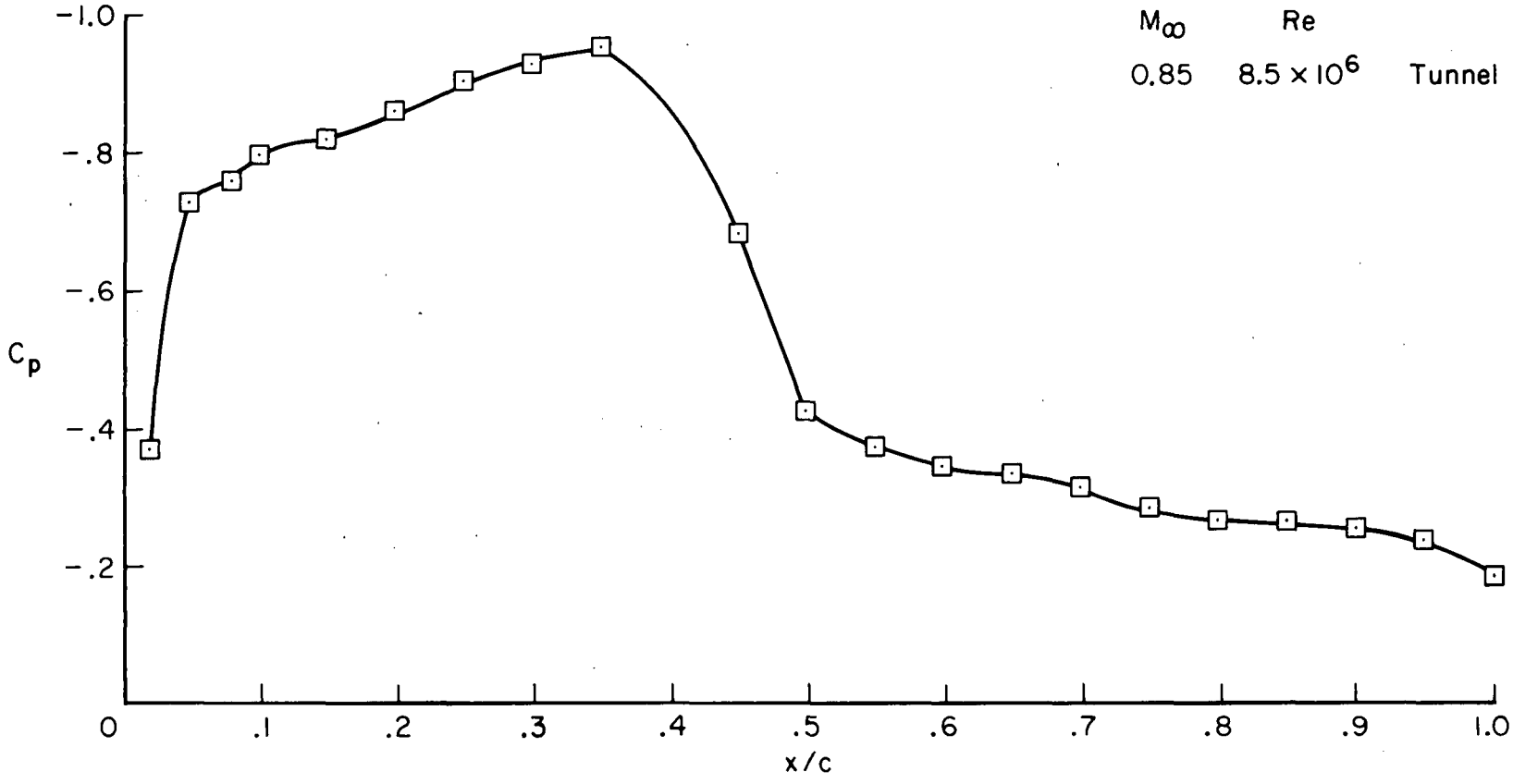

(b) Tunnel, $M_\infty = 0.85$.

Figure 8.– Concluded.

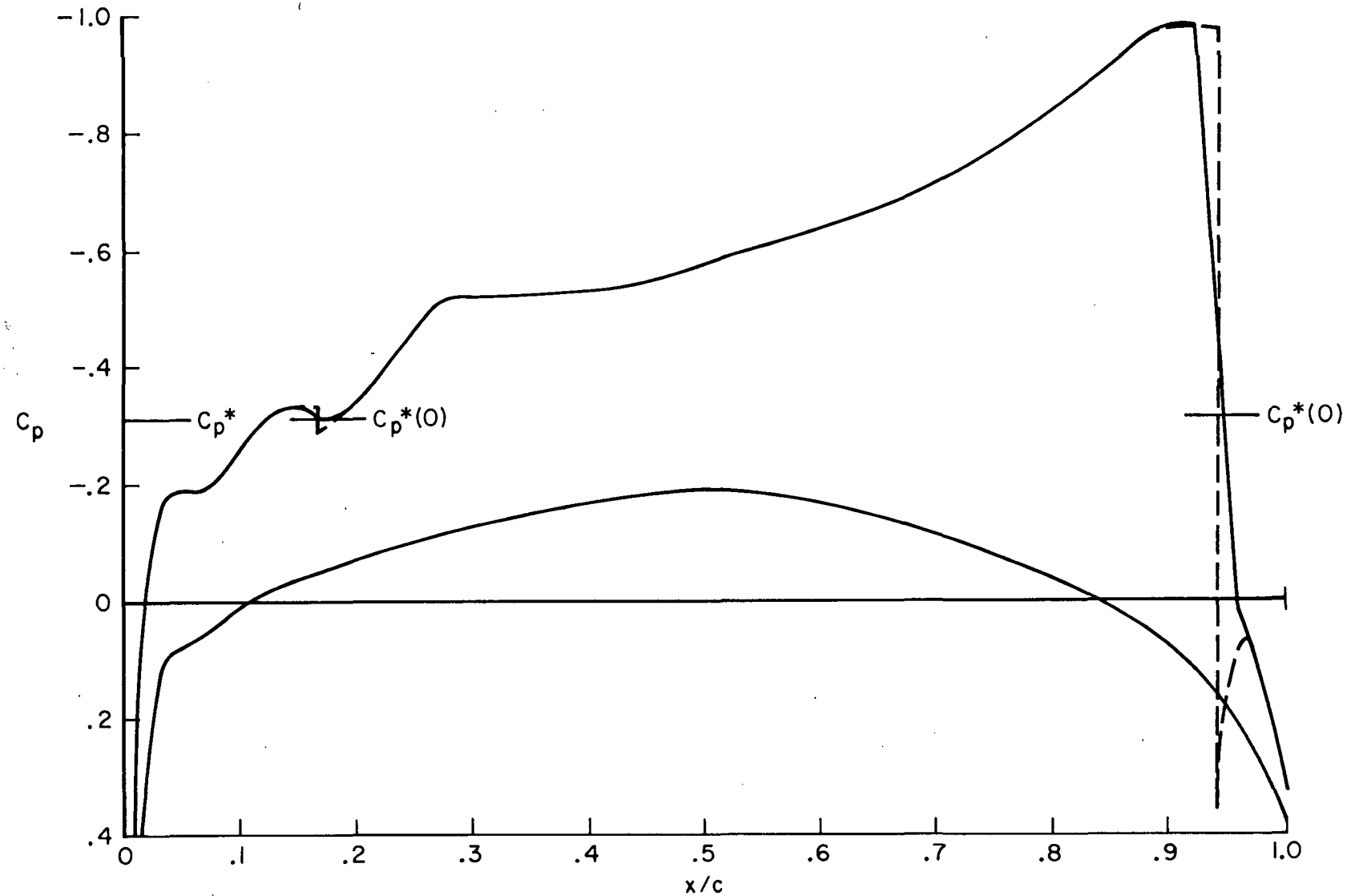

Figure 9.– Pressure coefficient at root section $M_\infty = 0.853$, coarse mesh.

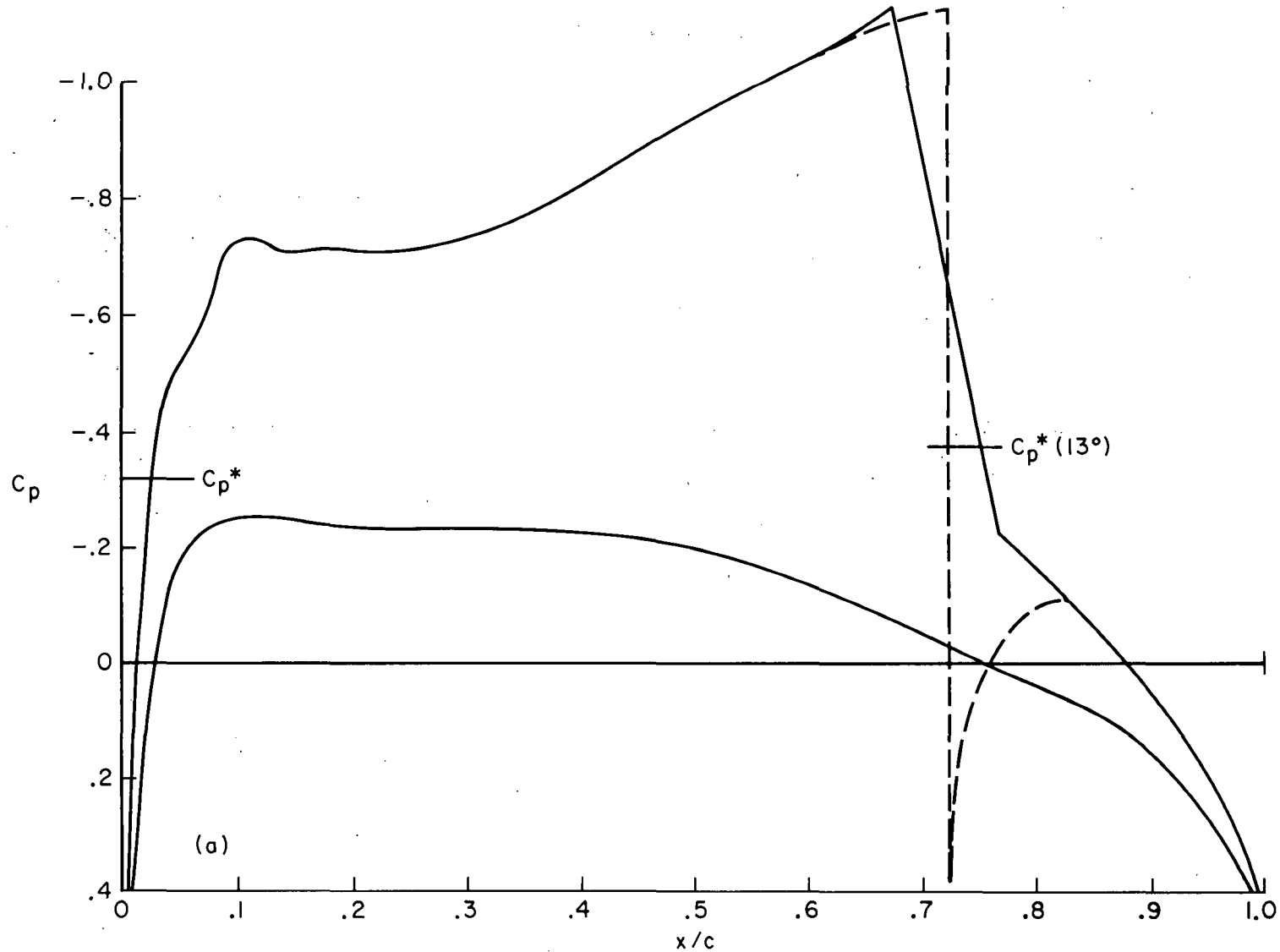

(a) $y/b = 0.553$

Figure 10.– Pressure coefficient at three successive spanwise mesh stations, $M_\infty = 0.853$ coarse mesh.

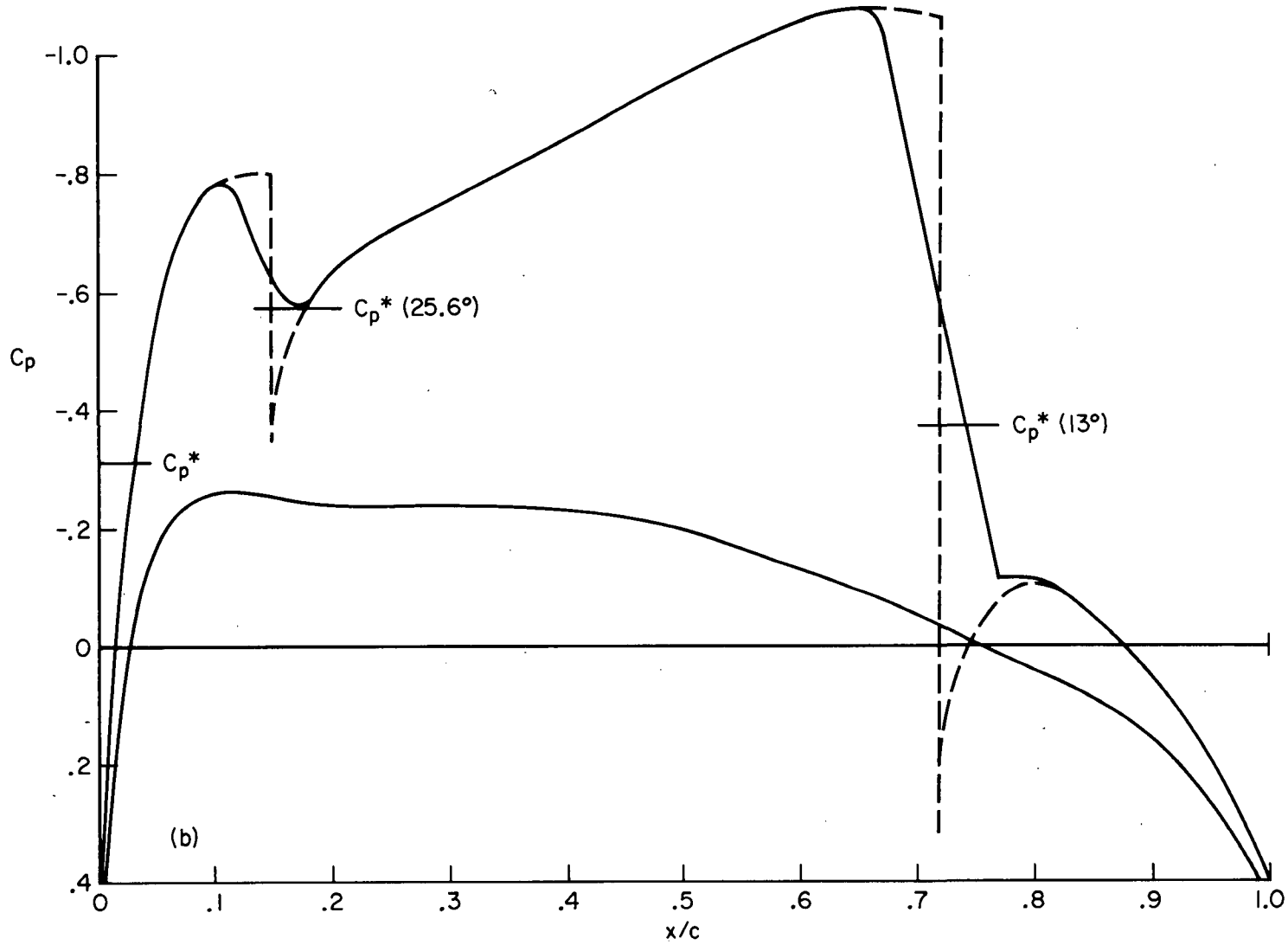

(b) $y/b = 0.623$

Figure 10.– Continued.

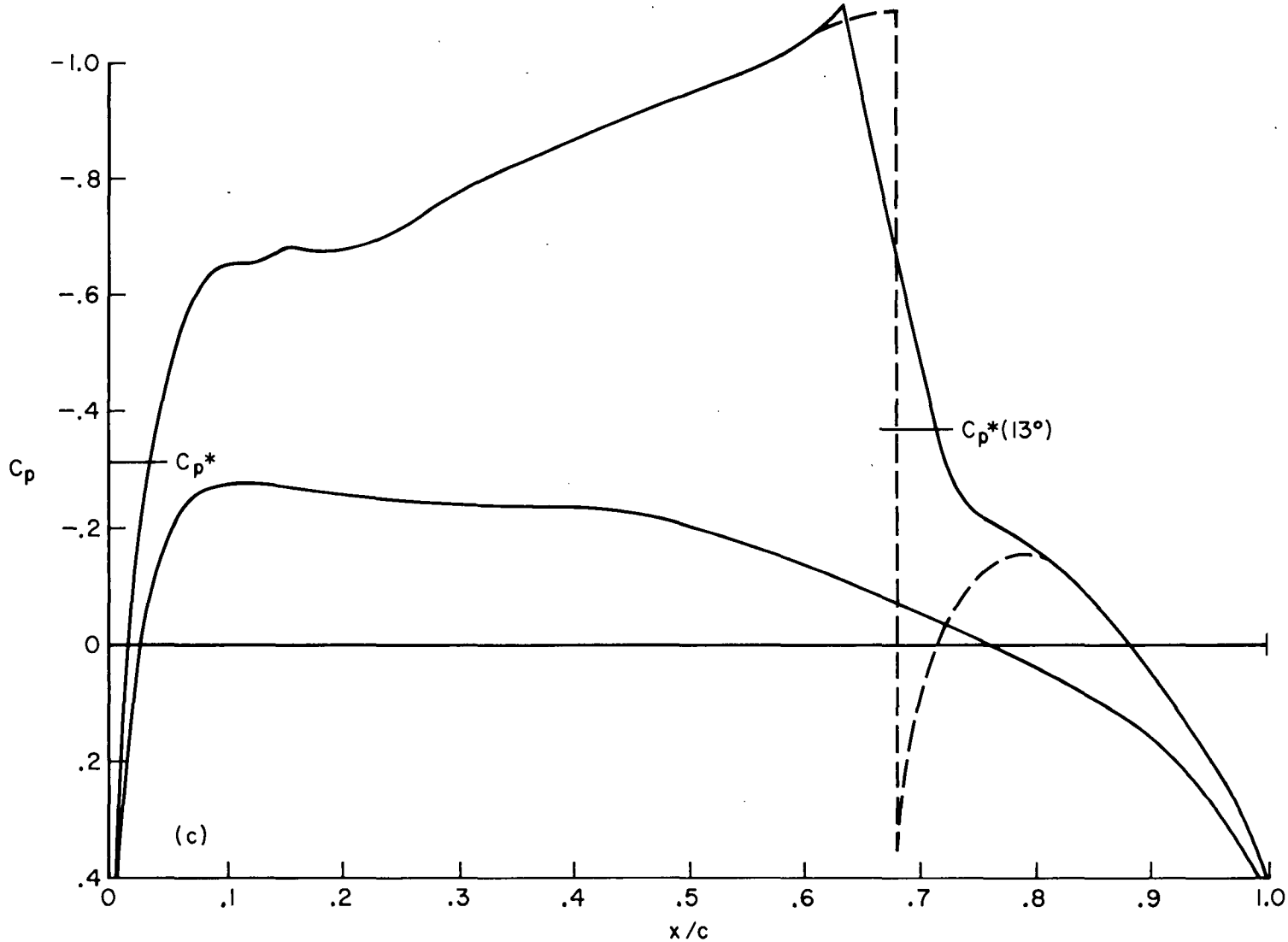

(c) $y/b = 0.693$.

Figure 10.– Concluded.

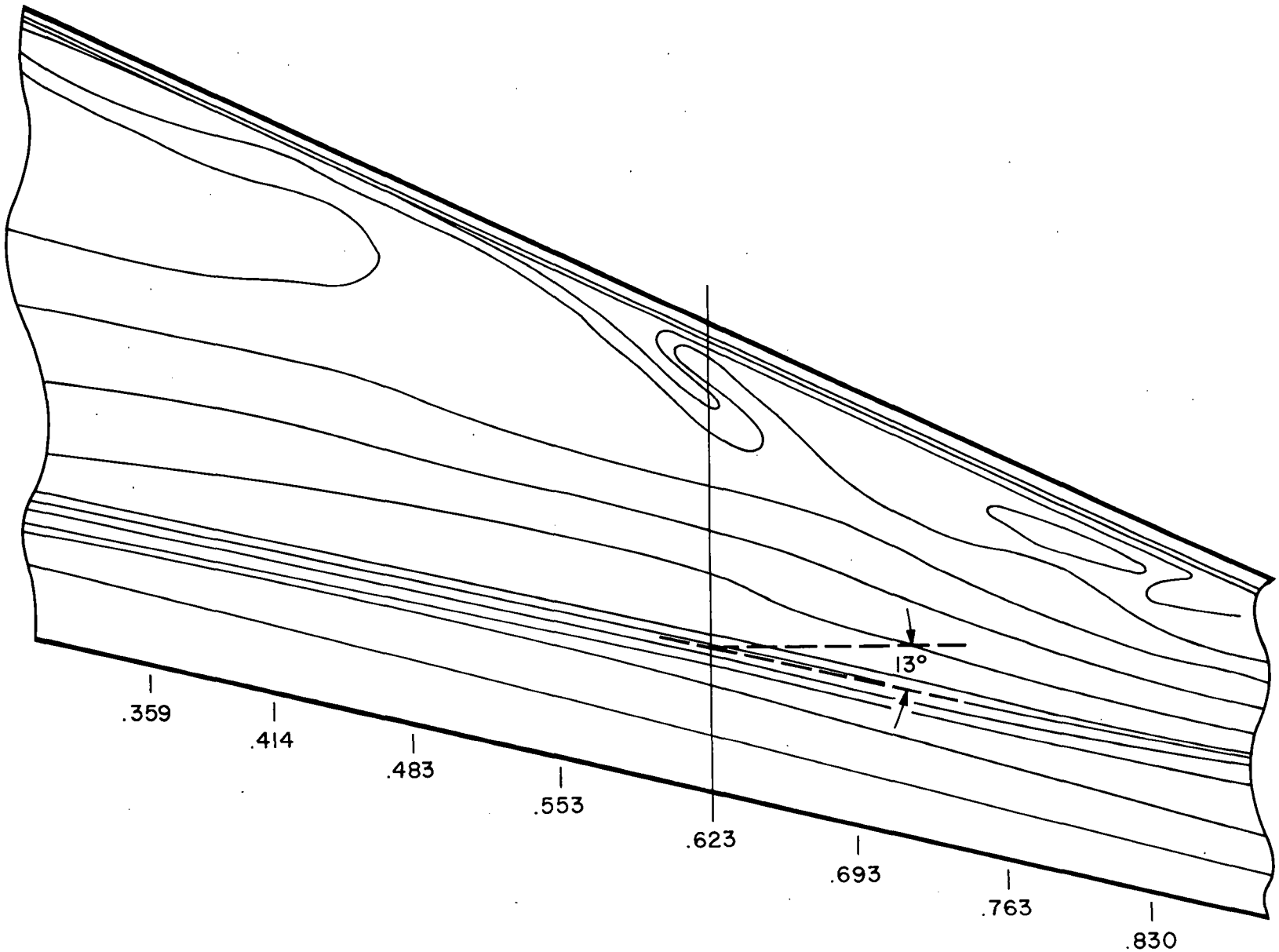

Figure 11.– Isobars for coarse mesh calculation, $M_\infty = 0.853$.

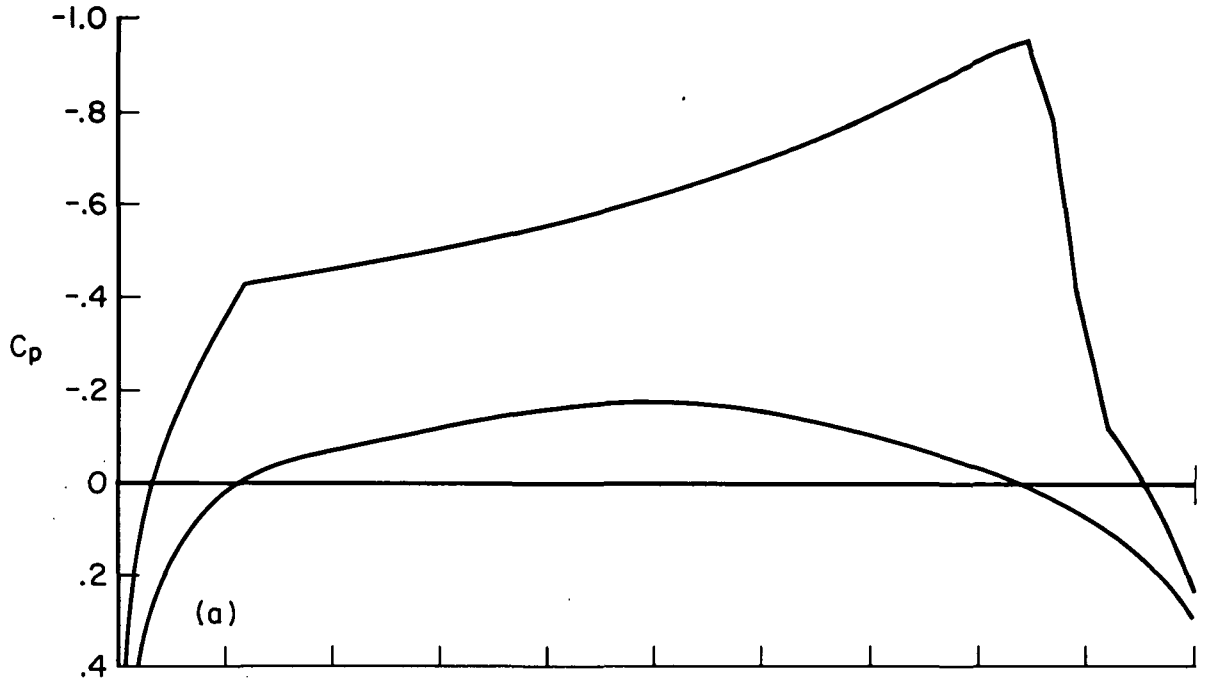

(a) $y/b = 0.0$

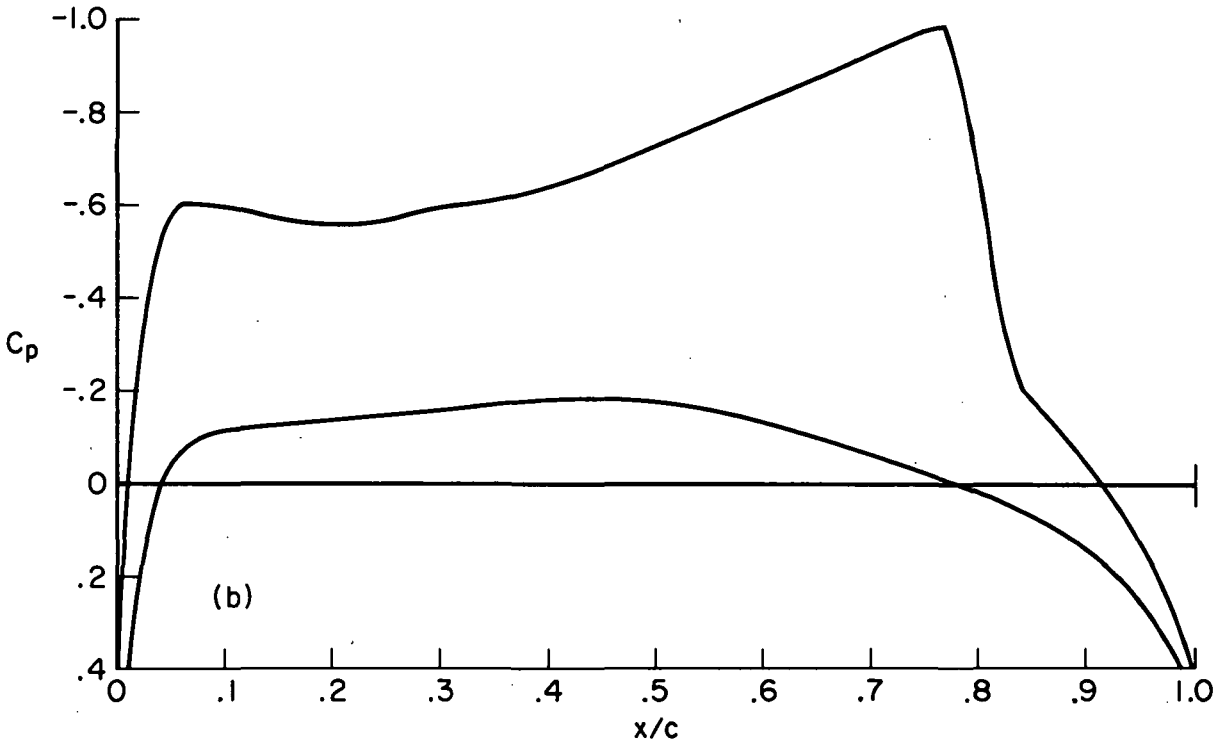

(b) $y/b = 0.1$

Figure 12.– Pressure coefficient at every fourth spanwise mesh station $M_\infty = 0.825$, fine mesh.

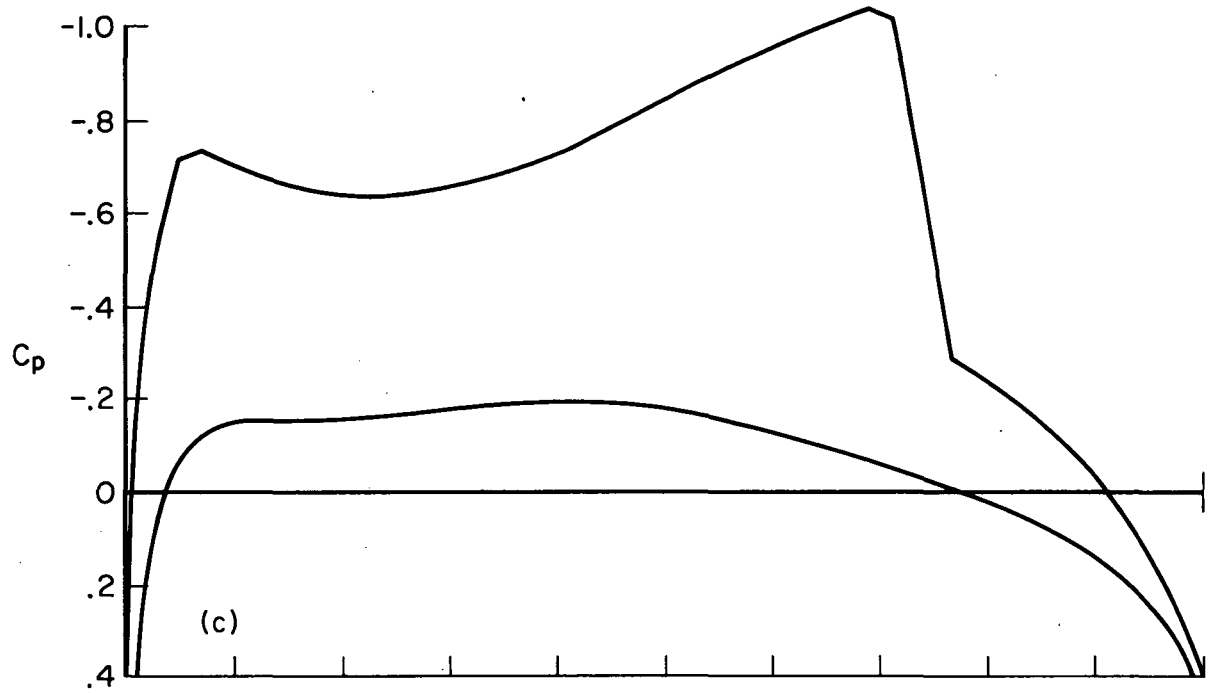

(c) $y/b = 0.2$

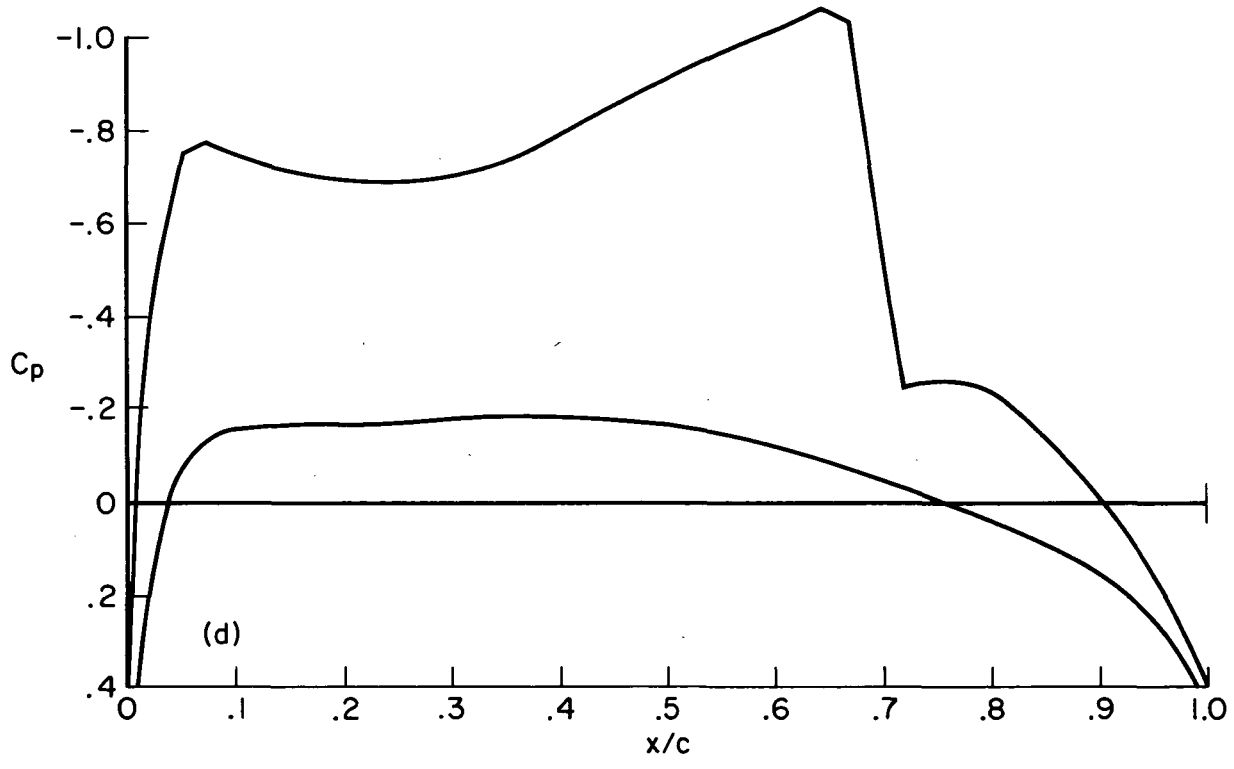

(d) $y/b = 0.3$

Figure 12.– Continued.

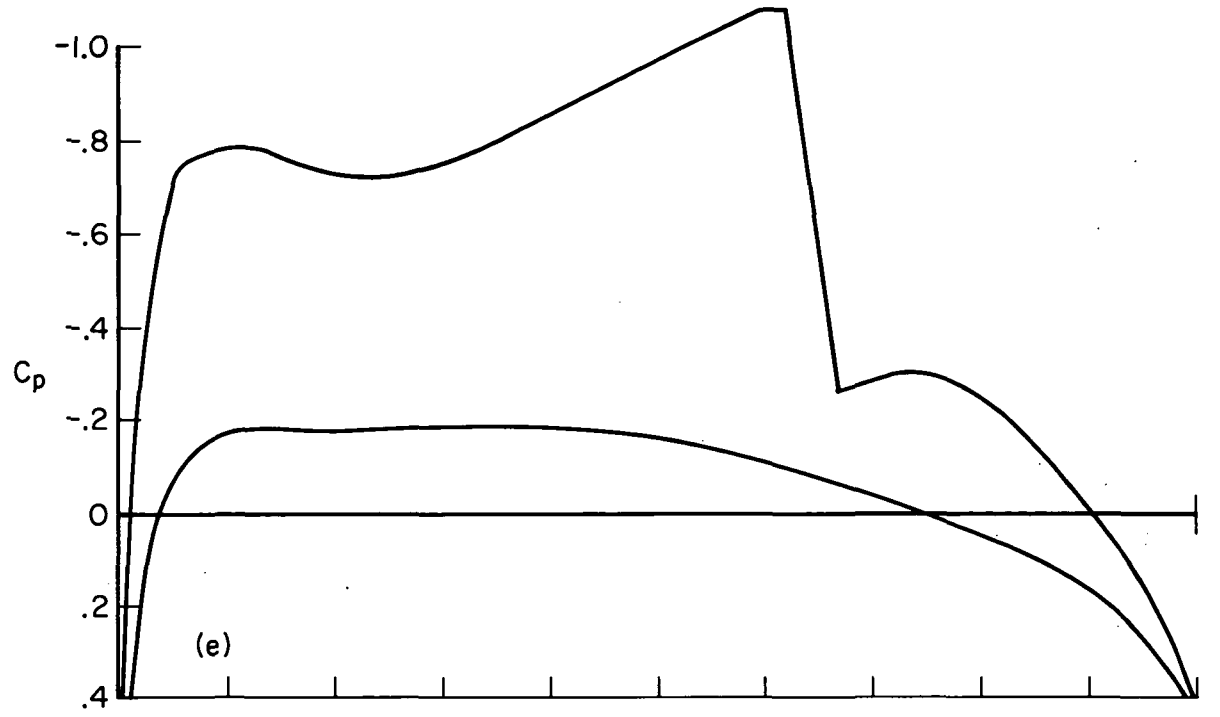

(e) $y/b = 0.4$

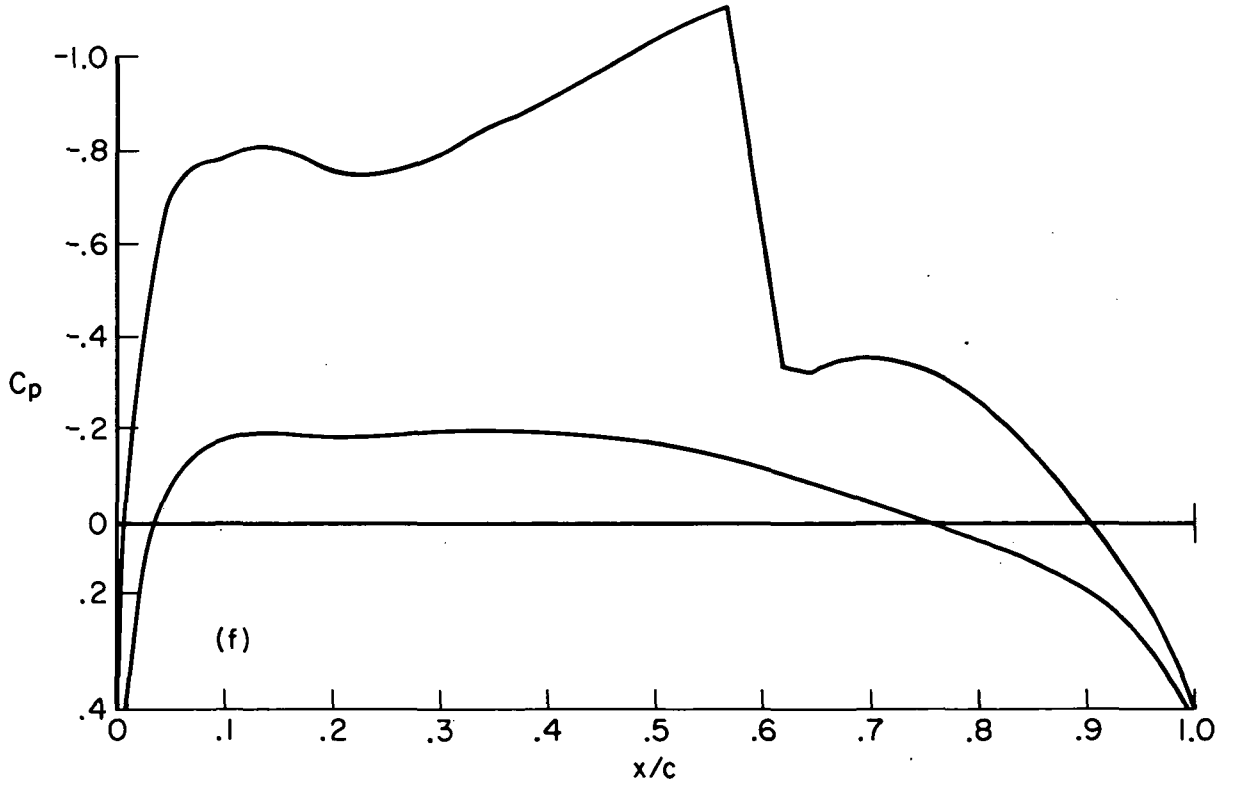

(f) $y/b = 0.5$

Figure 12.– Continued.

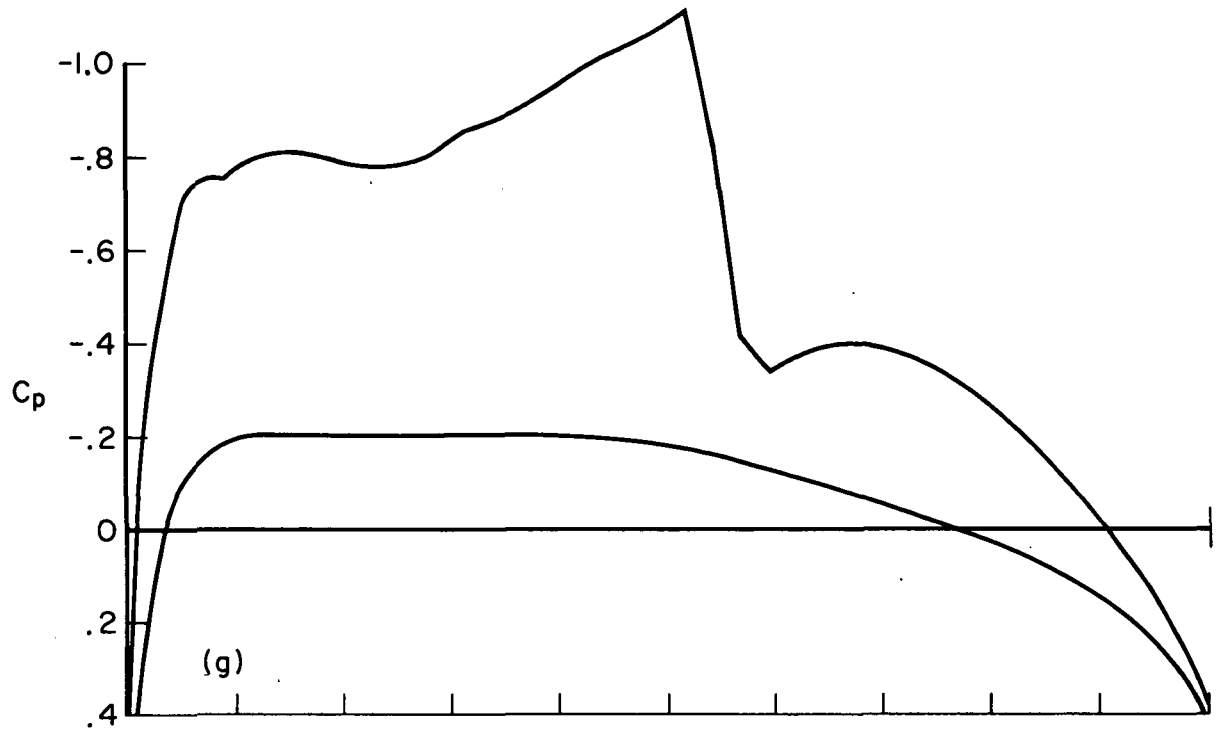

(g) $y/b = 0.6$

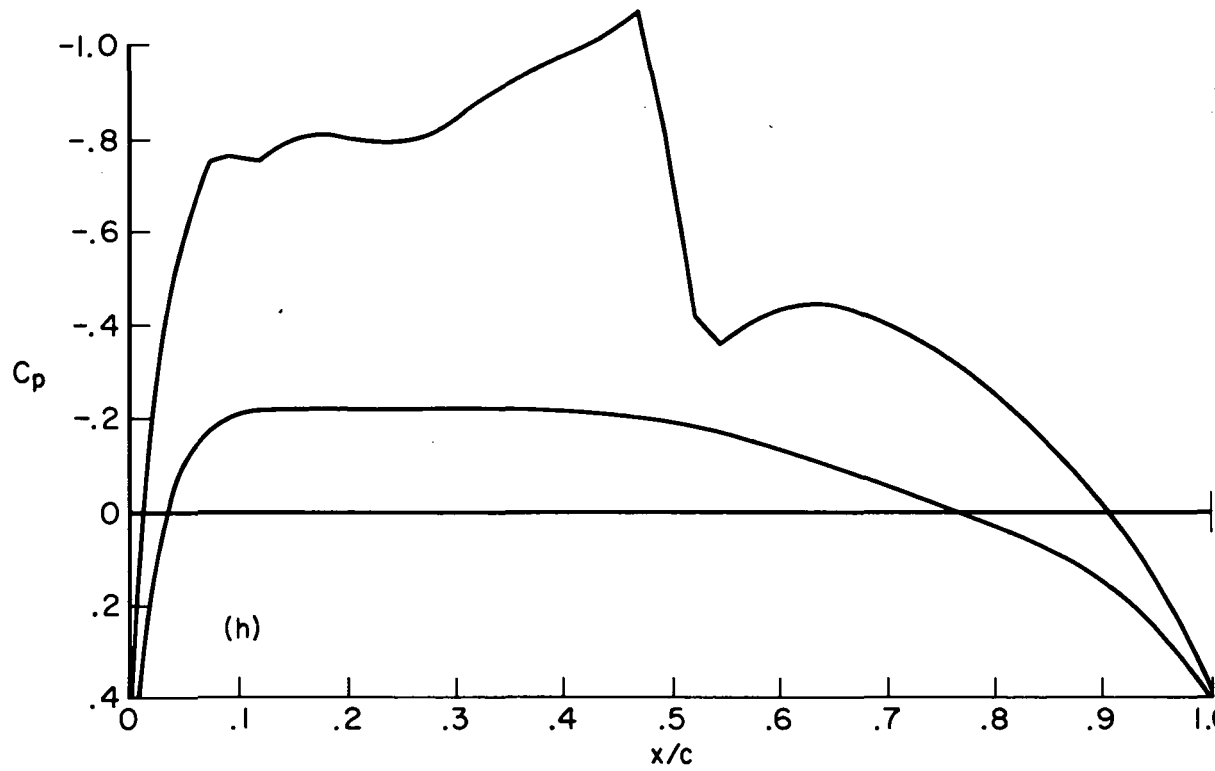

(h) $y/b = 0.7$

Figure 12.– Continued.

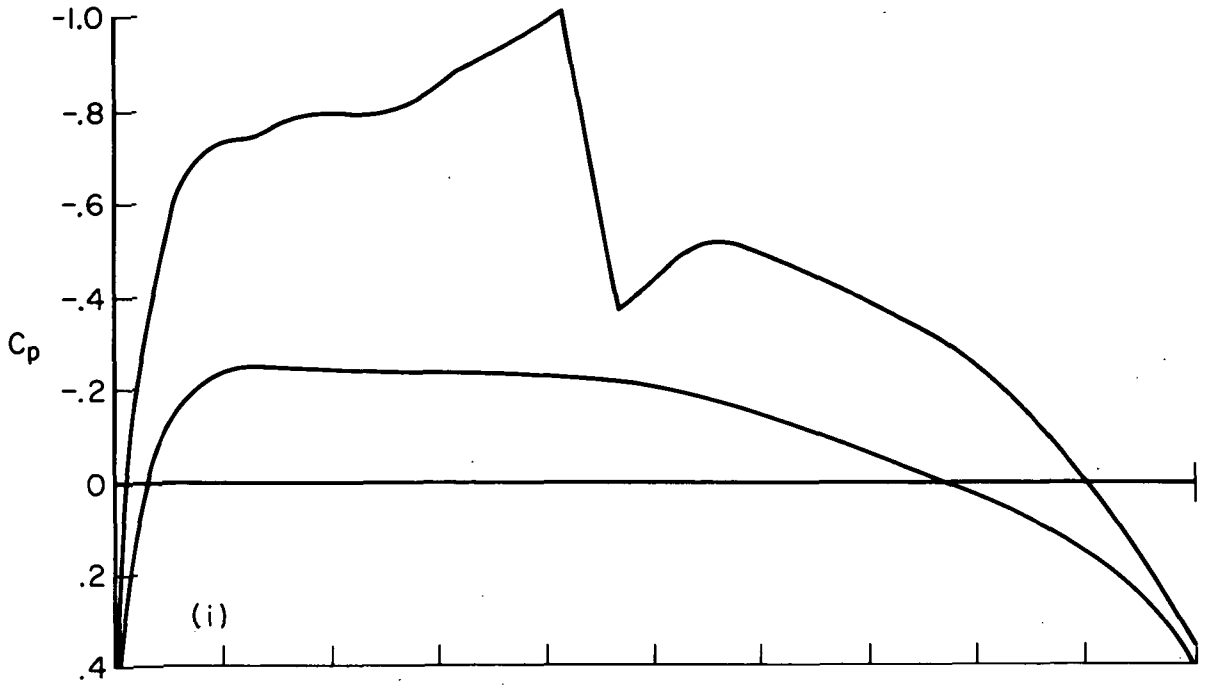

(i) $y/b = 0.8$

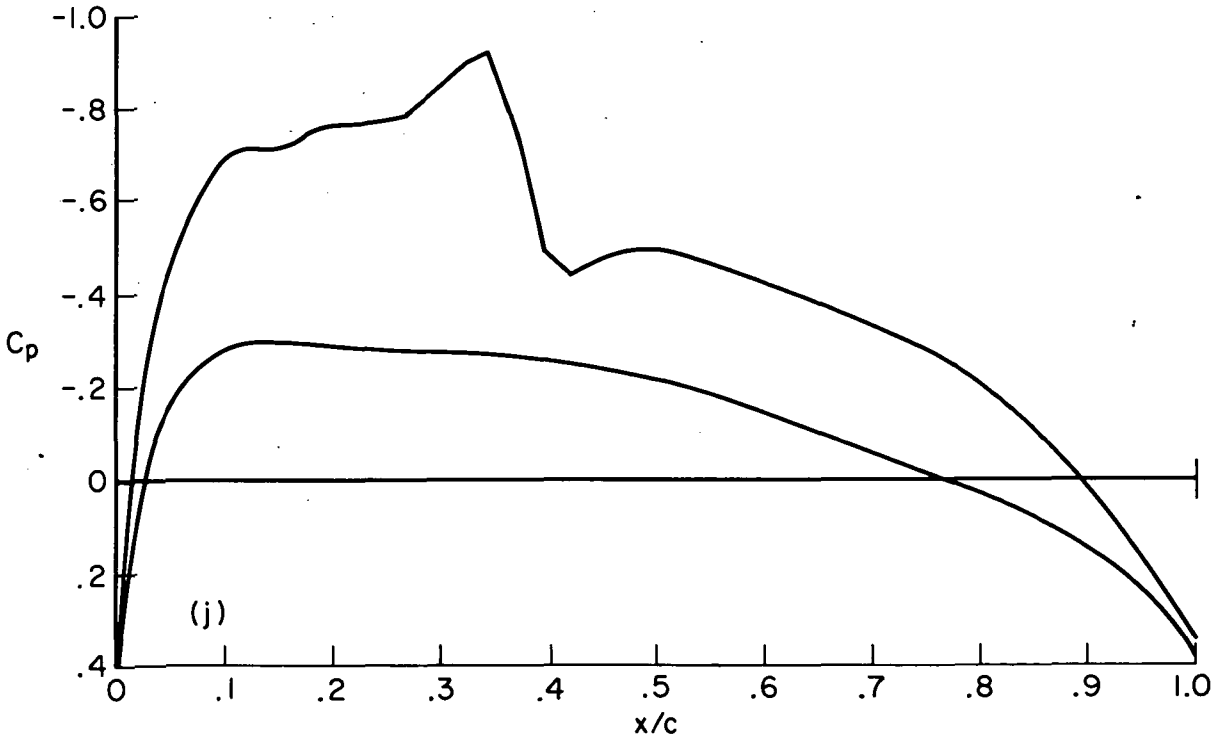

(j) $y/b = 0.9$

Figure 12.– Concluded.

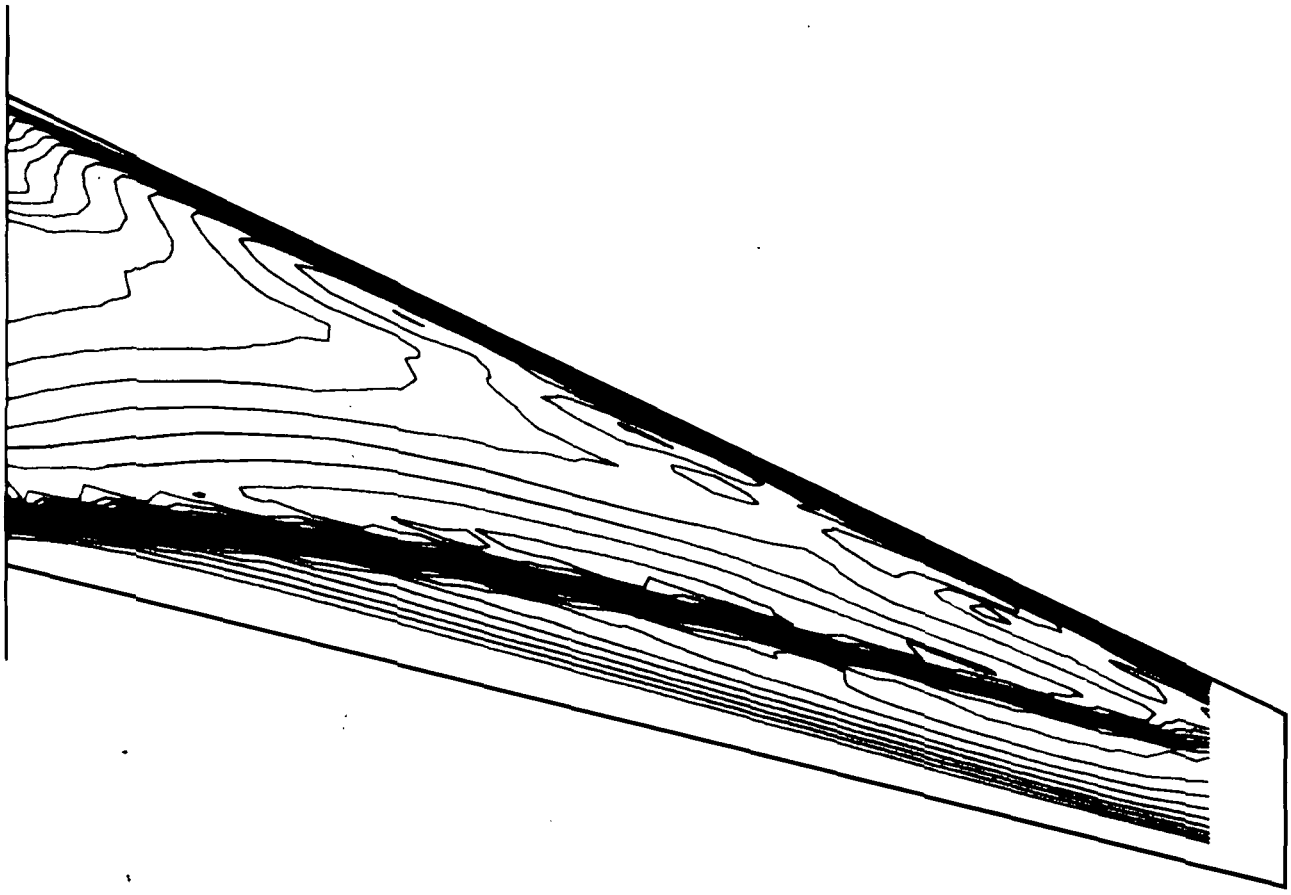

(a) Coarse mesh.

Figure 13.– Isobars for simulation of flow at $M_\infty = 0.825$.

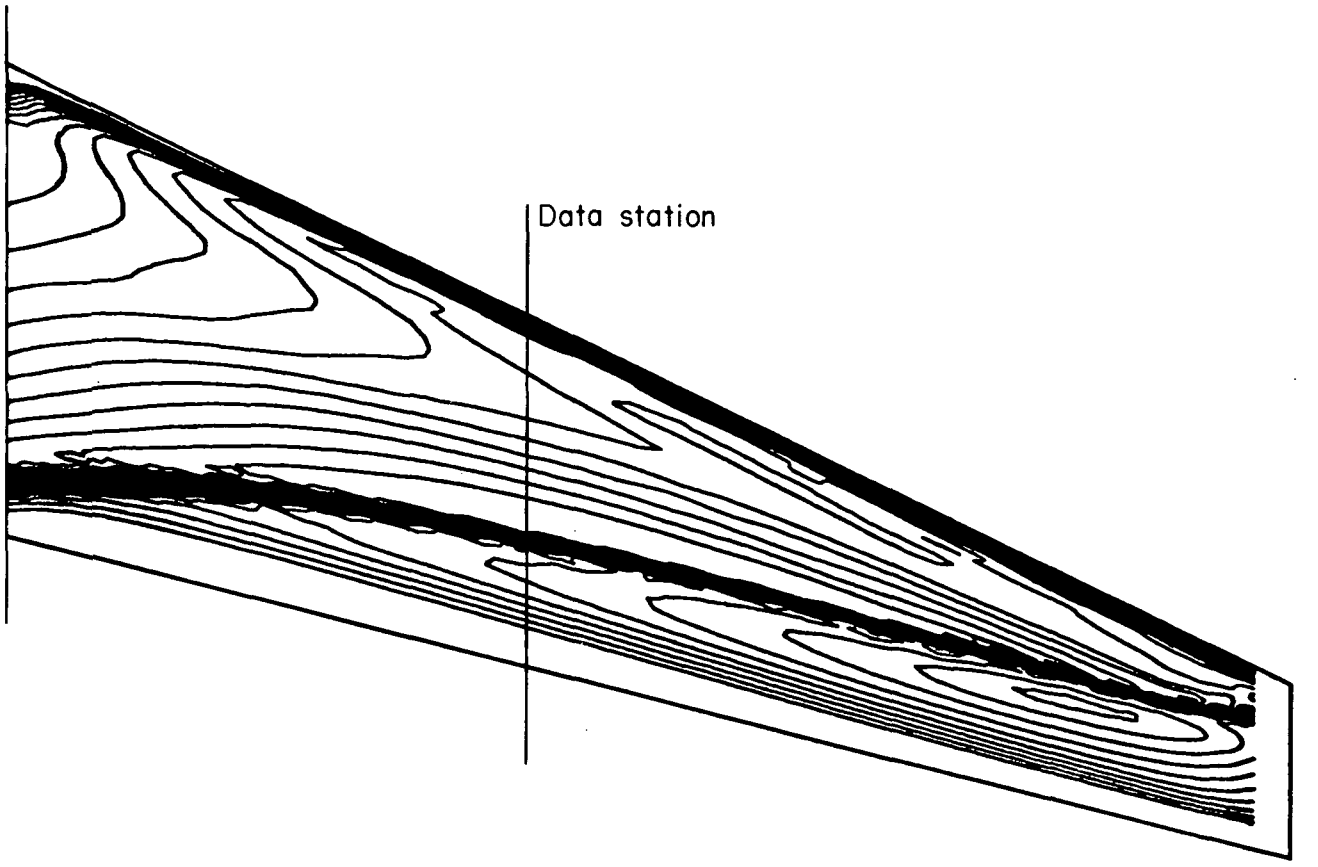

(b) Fine mesh.

Figure 13.– Concluded.

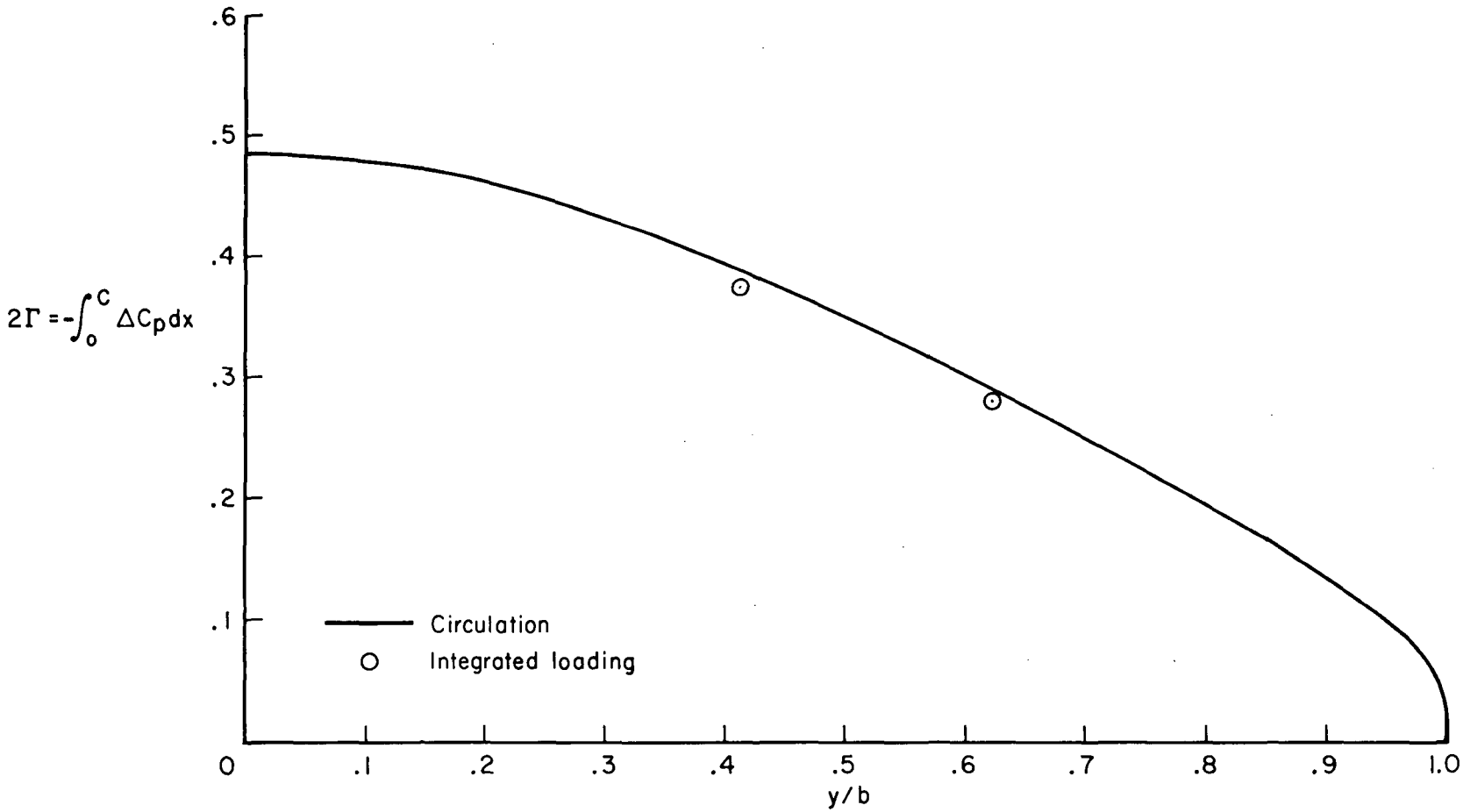

Figure 14.– Computed span loading on C-141 wing.

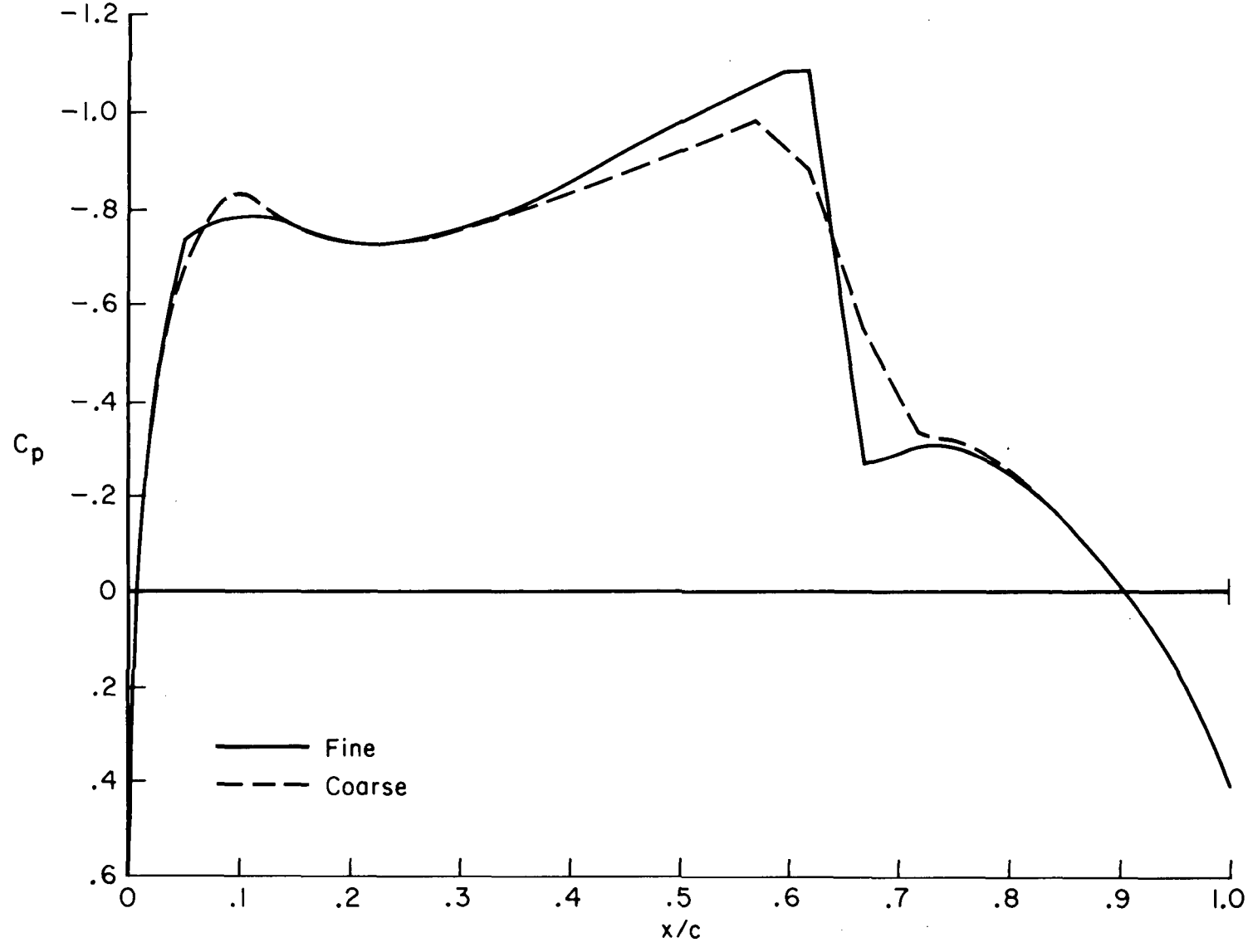

Figure 15.– Comparison of fine and coarse mesh calculations at $y/b \approx 0.4$ and $M_\infty = 0.825$.

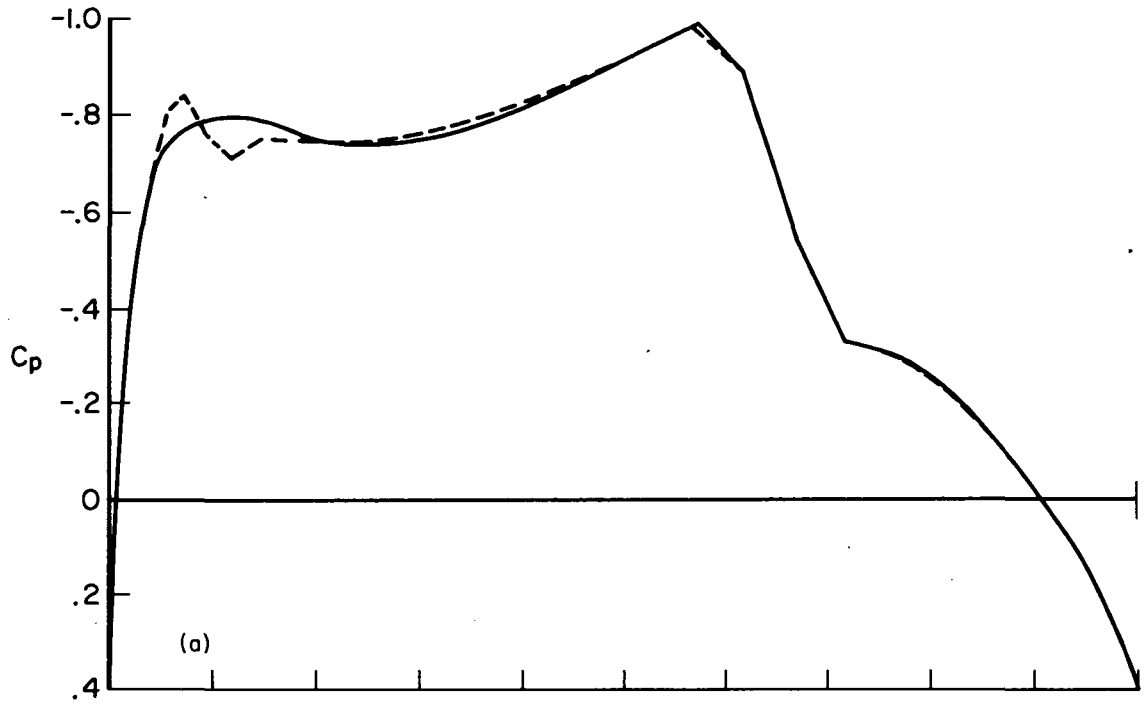

(a) Coarse mesh.

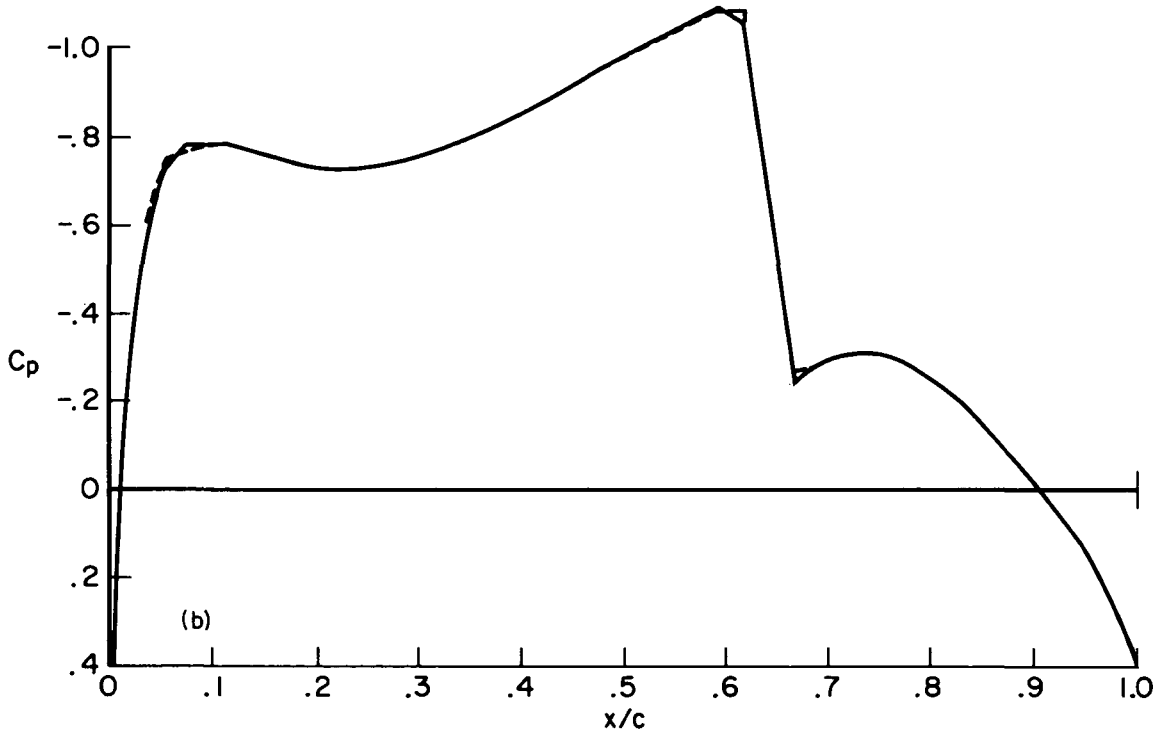

(b) Fine mesh.

Figure 16.– Comparison of two successive iterations in a fine and coarse mesh calculation $y/b \approx 0.4$ and $M_\infty = 0.825$.

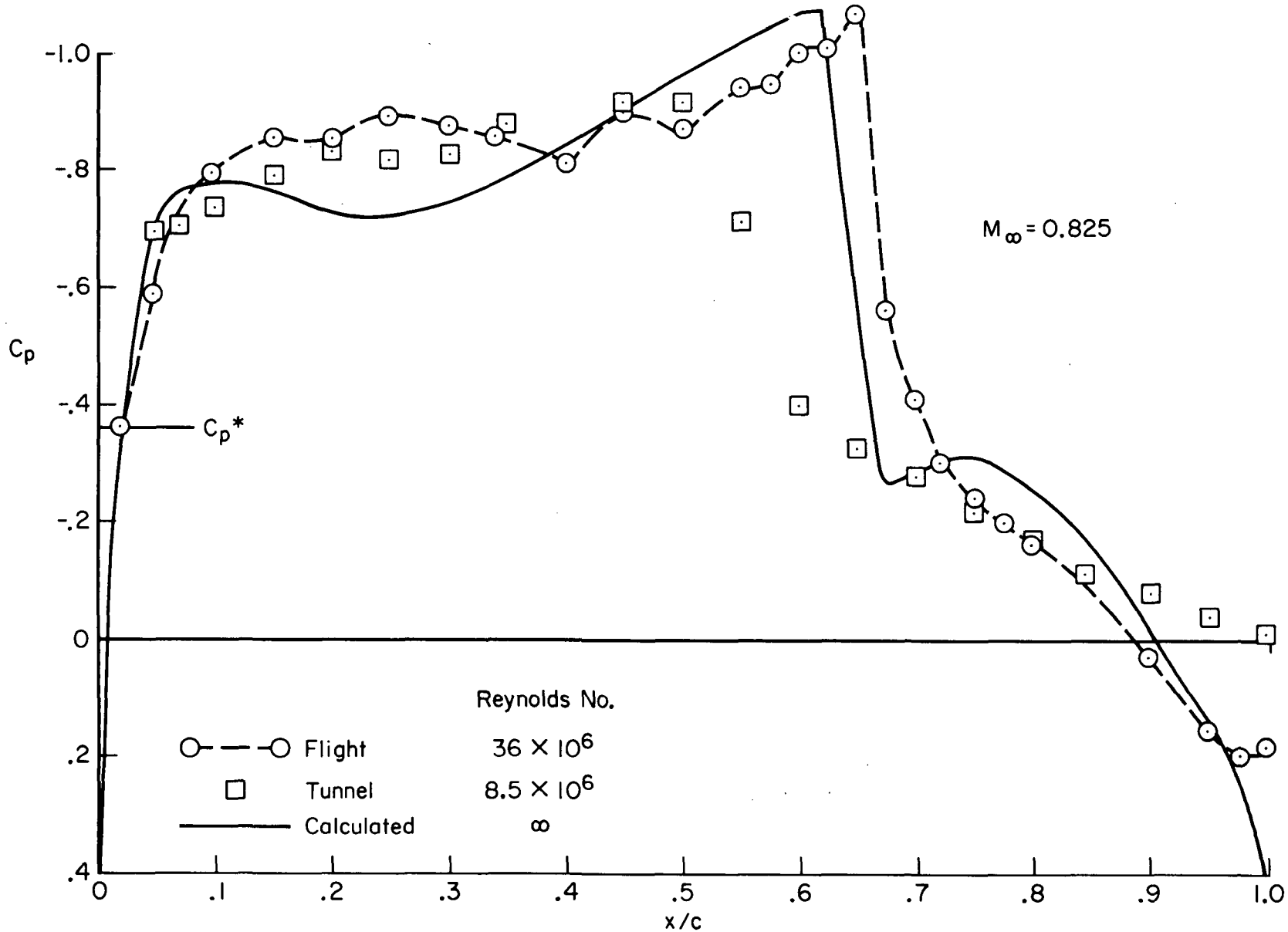

Figure 17.– Wind tunnel, flight, and computed (fine mesh) data for upper surface of wing at $y/b \approx 0.4$ and $M_\infty = 0.825$.

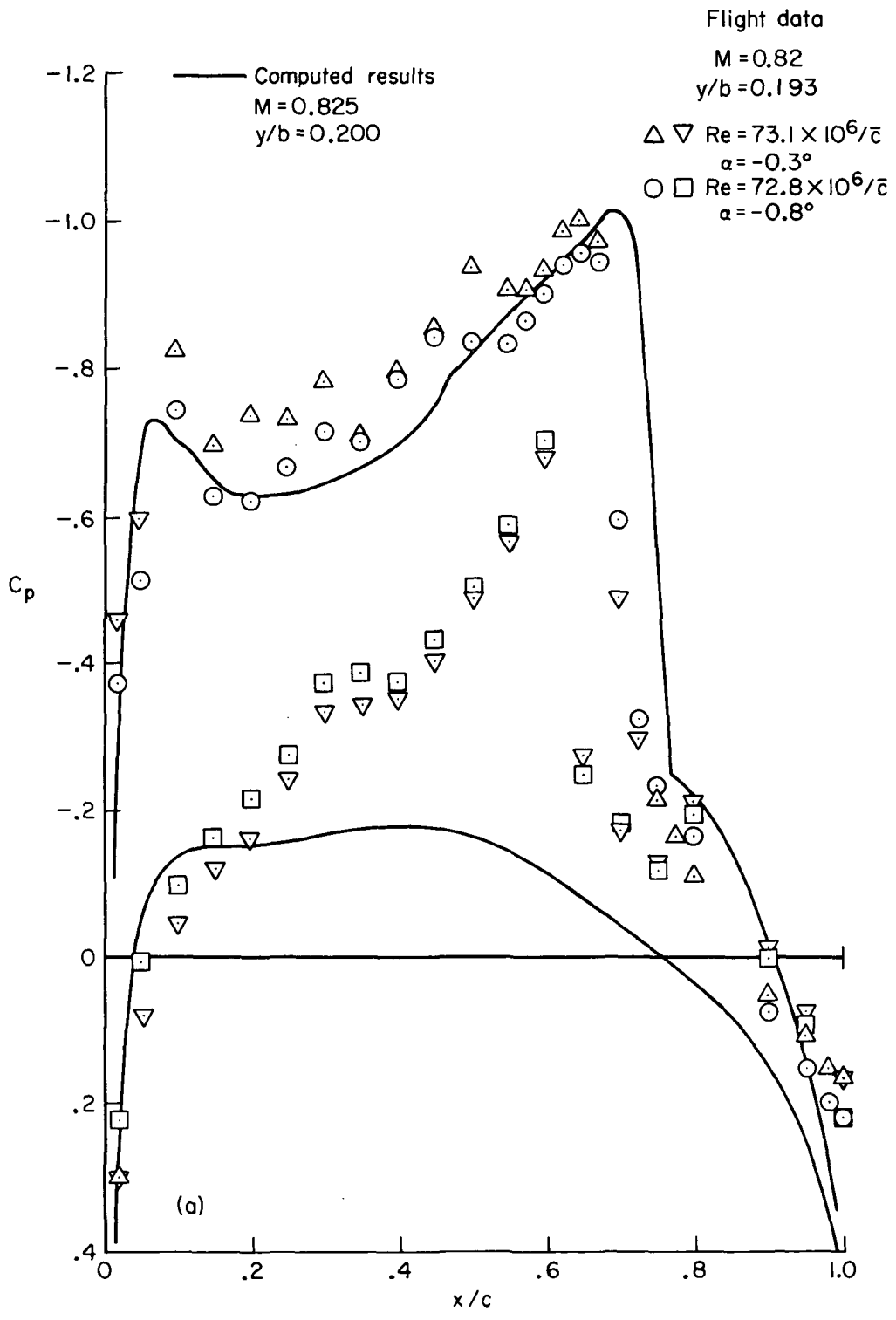

(a) $y/b \approx 0.2$

Figure 18.– Comparison of flight and computed (fine mesh) results at three span stations. Upper and lower surface included.

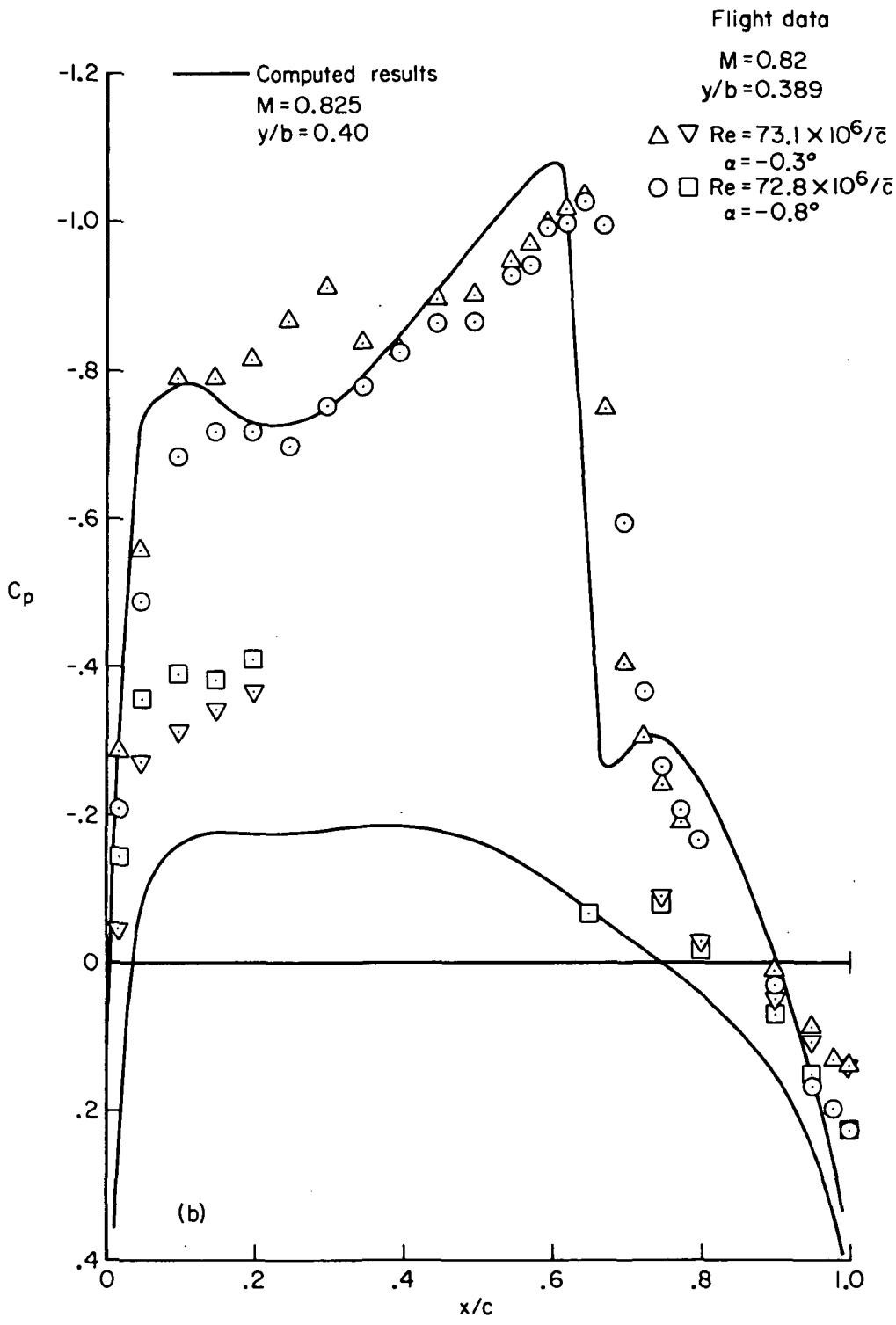

(b) $y/b \approx 0.39$

Figure 18.– Continued.

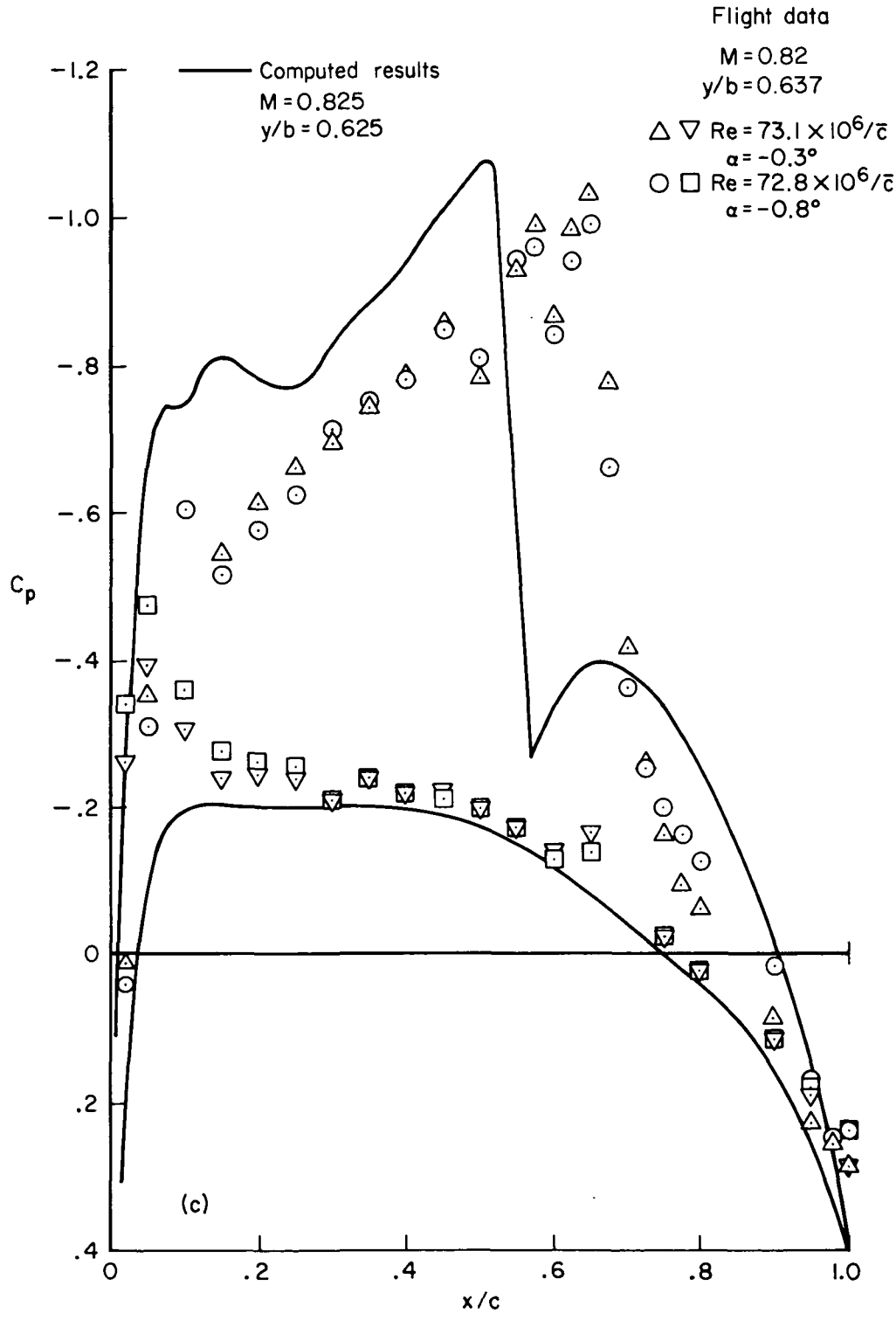

(c) $y/b \approx 0.63$.

Figure 18.– Concluded.

NASA-Langley, 1973 — 1 A–4583

NATIONAL AERONAUTICS AND SPACE ADMINISTRATION
WASHINGTON, D.C. 20546

OFFICIAL BUSINESS
PENALTY FOR PRIVATE USE $300

SPECIAL FOURTH-CLASS RATE BOOK

POSTAGE AND FEES PAID
NATIONAL AERONAUTICS AND SPACE ADMINISTRATION
451

U.S.MAIL

POSTMASTER: If Undeliverable (Section 158 Postal Manual) Do Not Return

"The aeronautical and space activities of the United States shall be conducted so as to contribute . . . to the expansion of human knowledge of phenomena in the atmosphere and space. The Administration shall provide for the widest practicable and appropriate dissemination of information concerning its activities and the results thereof."

—NATIONAL AERONAUTICS AND SPACE ACT OF 1958

NASA SCIENTIFIC AND TECHNICAL PUBLICATIONS

TECHNICAL REPORTS: Scientific and technical information considered important, complete, and a lasting contribution to existing knowledge.

TECHNICAL NOTES: Information less broad in scope but nevertheless of importance as a contribution to existing knowledge.

TECHNICAL MEMORANDUMS: Information receiving limited distribution because of preliminary data, security classification, or other reasons. Also includes conference proceedings with either limited or unlimited distribution.

CONTRACTOR REPORTS: Scientific and technical information generated under a NASA contract or grant and considered an important contribution to existing knowledge.

TECHNICAL TRANSLATIONS: Information published in a foreign language considered to merit NASA distribution in English.

SPECIAL PUBLICATIONS: Information derived from or of value to NASA activities. Publications include final reports of major projects, monographs, data compilations, handbooks, sourcebooks, and special bibliographies.

TECHNOLOGY UTILIZATION PUBLICATIONS: Information on technology used by NASA that may be of particular interest in commercial and other non-aerospace applications. Publications include Tech Briefs, Technology Utilization Reports and Technology Surveys.

Details on the availability of these publications may be obtained from:

SCIENTIFIC AND TECHNICAL INFORMATION OFFICE

NATIONAL AERONAUTICS AND SPACE ADMINISTRATION

Washington, D.C. 20546